UNIVERSITAT POLITÈCNICA DE CATALUNYA

Laboratory of Photonics
Electromagnetics and Photonics Engineering group
Dept. of Signal Theory and Communications

OPTICAL SOLITONS IN QUADRATIC NONLINEAR MEDIA AND APPLICATIONS TO ALL-OPTICAL SWITCHING AND ROUTING DEVICES

Autor: María Concepción Santos Blanco
Director: Lluís Torner

Barcelona, january 1998

Chapter 3

Solitons in Quadratic Nonlinear Media

After the revision just made about the basic concepts of light propagation and optical solitons in previous chapter the natural question arises about whether solitary wave propagation is possible inside a quadratic nonlinear crystal. Of course since the system is not integrable the *solitary waves* found if any, can not be considered *solitons* in a strict sense since they won't constitute a full decomposition of nonlinear modes of the system but still, if they are shown to arise from a wide range of input and system parameter conditions and to be stable and approximately keep their shape on propagation, can just the same be useful for practical applications adding the advantages of easy and cheap manufacturing and low power operation outlined in the introductory chapter. That is indeed the case for the solitary waves existing in quadratic nonlinear media. As customary, they have been taken to be called *solitons* in the knowledge that they are actually 'solitary waves'.

Numerical integration of equations (2.94) through standard beam propagation methods such for example the Split-step Fourier method whose basis where set in previous chapter and which has provided the outputs shown in Figure 3-1, can be used to obtain evidence on how the system seems to slowly tend towards a fully stationary state in a wide range of system parameters and input fields.

The clue on the existence of fully stationary wave modes in quadratic nonlinear materials

is given by the fact that a localized stationary solution to the system of equations (2.94) in analytic form was found by Yu. N. Karamzin and A. P. Sukhorukov in 1975 [80] for certain fixed values of *all* parameters in it thus constituting a *zero-parameter family* of stationary solutions to the system in (2.94).

Nowadays, it is known that this solution is a mere sample of a larger two parameter family of bright solitary wave solutions. The complete family of stationary solutions in the absence of walk-off was found numerically by Buryak and Kivshar [90]-[92] and by Torner [93]-[94] while experimental evidence of their existence in both planar waveguides and bulk media was reported by Torruellas et al. [103] and Schieck et al. [102] respectively.

This chapter is devoted to the search for stationary solutions of equations (2.94) making use of the basic properties of the system which also allow to elucidate the stability, and by means of numerical methods such as the *shooting* method. A discussion of the basic features of the stationary solutions found is carried out and the chapter is concluded with exploration of the dynamical regime and some considerations about excitation of solitary wave structures.

The following section analyses the system given by (2.94) and its basic properties to elucidate the best approach to follow for a wise search, while anticipating some results on the stability of the stationary solutions finally found through the numerics.

3.1 Search for stationary solutions

3.1.1 Search strategy

In a system such as the one analyzed here, two are basically the possibilities for the steady-state solutions, namely they can be oscillating solutions featuring a period in which the characteristics of the propagation are continuously repeated, or else they can be fully stationary meaning that all their parameters are constant on propagation. Here the analysis concentrates on the latter case corresponding to the solutions known to date.

Some considerations about the system properties need to be made in order to follow an appropriate and efficient search. First of all, the objects of the search are identified as *travelling*

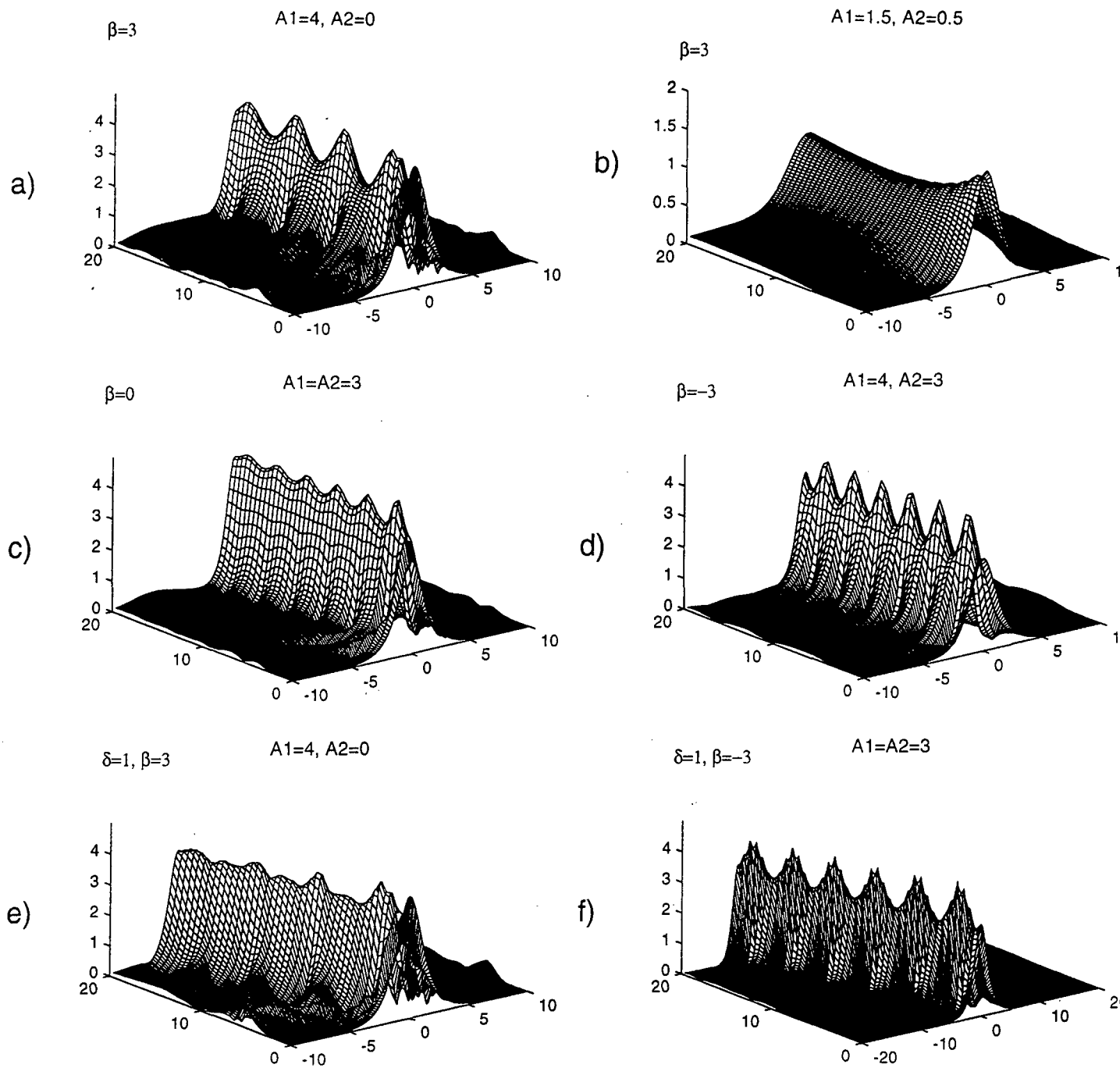

Figure 3-1: Examples of solitary wave propagation. Parameters are as in section 3.6. a): only FF input $\beta = 3$, $A_1 = 4$; b): low energetic soliton with $\beta = 3$, $A_1 = A_2 = 3$; c): $\beta = 0$, $\beta = -3$, $A_1 = 4$, $A_2 = 3$; d): negative β, $\beta = -3$, $A_1 = 4$, $A_2 = 3$; e) and f): examples with a non vanishing walk-off, $\delta = 1$; e): $\beta = 3$, $A_1 = 4$, $A_2 = 0$; f): $\beta = -3$, $A_1 = A_2 = 3$.

wave structures whose dependences with the free variables of the system must be in general

$$a_{1,2}(s,\xi) = U_{1,2}(s - v\xi)\exp(j\kappa_{1,2}\xi)\exp\left(j\phi_{1,2}(s - v\xi)\right), \tag{3.1a}$$

where all the functions in right hand side are real, s and ξ stand for the transverse and the propagation variable respectively, v gives the transverse velocity of the traveling wave and $\kappa_{1,2}$ are known as *nonlinear phase shifts* of each harmonic and contemplate variations with a nonlinear origin, i.e. power dependent, on the respective propagation constants. They are responsible for the phase-locking that allows linearly wavevector mismatched fundamental and second harmonic waves to accommodate their respective propagation constants to nonlinearly cancel the mismatch and travel together as a unit thus forming a solitary wave. That leads to a necessary requirement for a travelling wave object to be formed known as the *phase locking condition*, namely

$$2\kappa_1 - \kappa_2 + \beta = 0. \tag{3.2}$$

The parameter v in (3.1a) characterizes the transverse velocity with which a given traveling wave structure walks the propagation axis (the z axis throughout the present analysis) off. Interest is lied in solutions to the system defined by (2.94) which in addition to being travelling wave are *localized* structures, either bright or dark but always such that they feature a finite interval in the travelling wave variable where variations of the transverse derivatives are allowed, or in other words,

$$\frac{\partial^n}{\partial\eta^n}U \underset{|\eta|\longrightarrow\infty}{\longrightarrow} 0, \tag{3.3}$$

being $\eta = s - v\xi$ the travelling wave variable.

Recalling the hypothesis made to obtain equations (2.94) starting from the real electromagnetic light propagation problem, care should be taken when dealing with very fast transverse travelling objects, attending that the derivation assumed propagation had mainly the direction of the z axis. Therefore connection of the results to real physical phenomena will be restricted to reasonably small values of v.

Recall the energy exchange requirements derived in previous chapter for traveling wave

objects

$$2U_1^2U_2\sin\left(\triangle\psi\right) = -\left(\left(r\psi_{1_s}+v\right)U_1^2\right)_s, \tag{3.4}$$

$$2U_1^2U_2\sin\left(\triangle\psi\right) = \left(\left(\alpha\psi_{2_s}+\left(\delta+v\right)\right)U_2^2\right)_s, \tag{3.5}$$

where connection with the functions in the ansatz (3.1a) is made through $\psi = \kappa\xi + \phi\left(\eta\right)$.

As the simplest way in which the energy exchange requirements are fulfilled assume both sides of equalities (3.4), (3.5) are zero meaning total absence of local energy exchanges. Regarding the left hand side term, that implies

$$\triangle\psi = \left(2\kappa_1 - \kappa_2 + \beta\right)\xi + 2\phi_1 - \phi_2 = 0, \tag{3.6}$$

which adds to the necessary phase-locking requirement the assumption that the fundamental phase profile doubles that for the second harmonic in all points of the transverse profile, i.e.

$$2\phi_1 = \phi_2. \tag{3.7}$$

As for cancellation of the right hand side terms in (3.4-3.5), the simplest solution considers purely tilted phase fronts verifying

$$\psi_{1_s} = \phi_{1_s} = -\frac{v}{r}, \tag{3.8}$$

$$\psi_{2_s} = \phi_{2_s} = -\frac{\left(v+\delta\right)}{\alpha}. \tag{3.9}$$

Applying to this result that in (3.7), it is obtained

$$v = \frac{r\delta}{2\alpha - r}, \tag{3.10}$$

which in the spatial case, i.e. $r = -1$, $\alpha \simeq -0.5$, gives in the presence of walk-off extraordinarily big values for the transverse soliton velocity which lack any physical meaning. Hence it is concluded that in the presence of walk-off solutions with the form (3.15) are not possible whereupon in the analysis it is set $\alpha = -0.5$ and $\delta = 0$.

Since in that case the formal problem does not depend upon the specific position in the

transverse coordinate from where one looks at it, it follows naturally that if $f(s,\xi)$ is a stationary solution with the form (3.15) then so is $f((s-\sigma),\xi)$, with σ any real value, meaning that the same solitary wave solution, or more specifically, the same stationary transverse amplitude and phase profile can be found travelling in any direction inside the crystal. That is expressed formally through the fact that under the conditions stated the parameter giving the transverse velocity, v, becomes arbitrary indicating that all solitary wave solutions obtained through this approach can be found traveling in any transverse direction, provided the proper excitation conditions are supplied.

Hence the search shall concentrate in purely tilted phase fronts solutions which in the spatial case require $\delta = 0$. The ansatz reads

$$a_{1,2}(s,\xi) = U_{1,2}(s - v\xi)\exp(j\kappa_{1,2}\xi)\exp\left(-j\mu_{1,2}(s - v\xi)\right), \tag{3.11a}$$

where $\mu_2 = 2\mu_1 = 2v$ are the constants characterizing the linear tilt. Given the special transverse phase dependence of these solutions and for the sake of a more direct relation between formal parameters and experimental measurements, it is usual to redefine the nonlinear phase shift constants so that they retain all dependences with the propagation coordinate as follows

$$\overline{\kappa}_{1,2} = \kappa_{1,2} + \mu_{1,2}v. \tag{3.12}$$

Specifically for each nonlinear phase shift constant the equivalences are

$$\overline{\kappa}_1 = \kappa_1 - \frac{v^2}{r}, \tag{3.13}$$

$$\overline{\kappa}_2 = \kappa_2 - v\frac{(v+\delta)}{\alpha}. \tag{3.14}$$

Using this redefinitions of the nonlinear phase shifts, the ansatz for the solutions searched for is

$$a_{1,2}(s,\xi) = U_{1,2}(s - v\xi)\exp(j\overline{\kappa}_{1,2}\xi)\exp\left(-j\mu_{1,2}s\right). \tag{3.15}$$

Equalities (2.119),(2.120) provide the equations that allow to numerically search for the

stationary solutions. Recalling that $\psi_\xi = \kappa - v\phi_s$ one has

$$\frac{r}{2}U_{1ss} + \left(\kappa_1 - v\phi_{1_s} - \frac{r}{2}\left(\phi_{1_s}\right)^2\right)U_1 - U_1U_2 = 0, \tag{3.16}$$

$$\frac{\alpha}{2}U_{2ss} + \left(\kappa_2 - (v+\delta)\,\phi_{2_s} - \frac{\alpha}{2}\left(\phi_{2_s}\right)^2\right)U_2 - U_1^2 = 0, \tag{3.17}$$

which generically can be written

$$\frac{r}{2}U_{1ss} + \gamma_1 U_1 - U_1U_2 = 0, \tag{3.18}$$

$$\frac{\alpha}{2}U_{2ss} + \gamma_2 U_2 - U_1^2 = 0.$$

Using (3.8), (3.9) the parameters γ_1 and γ_2 in the equations are related to those in the ansatz (3.1a) through

$$\gamma_1 = \kappa_1 - \frac{v^2}{2r} = \overline{\kappa}_1 + \frac{3}{2}\frac{v^2}{r}, \tag{3.19}$$

$$\gamma_2 = \kappa_2 + \frac{(v+\delta)^2}{2\alpha} = \overline{\kappa}_2 + \frac{3}{2}\frac{v\,(v+\delta)}{2\alpha} + \frac{\delta\,(v+\delta)}{2\alpha}. \tag{3.20}$$

Once the values of r and α for a specific configuration are set, the nonlinear problem parameters γ_1 and γ_2 which are connected for each value of β through

$$\gamma_2 = 2\gamma_1 + \beta, \tag{3.21}$$

parametrize the stationary solutions.

For the spatial case, $\delta = 0$ and v becomes an arbitrary parameter which is usually set to zero, whereupon it is a common practice to identify $\gamma_1 = \kappa_1$, $\gamma_2 = \kappa_2$.

Notice that for each $\chi^{(2)}$ sample β is fixed. Therefore solutions to (3.18) constitute a one parameter family. Mathematically the parameter is κ_1, while physically it may be identified as the total energy flow I.

In the analogy with $\chi^{(3)}$ solitons, defined by two parameters, width and velocity, one needs to consider that under the assumptions of non-local energy exchange, the velocity of the soliton became in the spatial case an arbitrary parameter leaving only one parameter to define the soliton family.

Finally as a brief summary of the findings throughout this section, consideration of the simplest way in which the energy equilibrium requirement stated in (3.4-3.5) is fulfilled, namely $\Delta\psi = 0$, in the spatial case only allows obtention of solitary wave solutions when no walk-off is present and in that case the solutions must have constant phase fronts $\phi_{1_s} = \mu_1$, $\phi_{2_s} = \mu_2$ such that $\mu_2 = 2\mu_1$.

3.1.2 Similarity rules

Great simplification to the obtention and analysis of solutions to equations (3.18) is achieved by noticing that they are invariant under the similarity transformations

$$\begin{aligned} \kappa_1 &\longrightarrow \mu\kappa_1, \quad \beta \longrightarrow \mu\beta, \quad U_1 \longrightarrow \mu U_1, \\ U_2 &\longrightarrow \mu U_2, \quad s \longrightarrow s/\sqrt{\mu}, \quad I \longrightarrow \mu^{3/2} I, \end{aligned} \tag{3.22}$$

with μ an arbitrary parameter. That entails that the soliton solutions may be transformed into each other following such rules.

This self-similarity has important consequences, from a formal point of view it helps to numerically solve equations (3.18) in an efficient way while physically it states that at either side of the phase matching the solutions are similar among them. Likewise it implies that at exact phase matching ($\beta = 0$) all the solitons existing in the absence of Poynting vector walk-off are self-similar so that in particular they feature a constant amplitude$\times$ (width)^2 relation.

3.1.3 The shooting method

The known analytical form of the zero-parameter solution to the equations (3.18) is

$$\begin{aligned} a_1(s) &= 3\sqrt{\alpha r}Sech^2(s), \\ a_2(s) &= -3rSech^2(s), \end{aligned} \tag{3.23}$$

and only occurs for fixed values of the equation parameters, i.e. $\beta = -2(\alpha - 2r)$, $\kappa_1 = -2r$ provided $\alpha r > 0$. It does not exhaust the whole soliton like behavior that the equations contain, but rather it may be completed by other bright solutions to the system which in every physical setting with its particular β value have different κ_1 values which are eventually chosen by the dynamics thus defining a one-parameter family of solitons for each different β.

Notice that by use of the similarity rules (3.22), the solution in (3.23) defines a point in the families of stationary bright solutions for any negative value of β given by

$$\beta = \mu\beta^a, \tag{3.24}$$

$$\kappa_1 = \mu\kappa_1^a, \tag{3.25}$$

$$a_i(s) = \mu a_i^a(s/\sqrt{\mu}), \tag{3.26}$$

where the superindex labels quantities related to the analytic solution. The family is completed by solutions for other values of κ_1.

This section concentrates on finding by numerical means the families of stationary bright profiles of the system given by (2.94) in the absence of Poynting vector walk-off employing a *shooting method* [138].

Given a system of equations, the shooting method builds up the families of solutions which adjust to some given characteristics through adequate selection of the initial conditions imposed to numerically integrate the equations. To this aim the parameters defining the initial conditions which graphically are considered to point at a certain location in the search parameters space, are systematically varied in successive numerical integrations. From the set of solutions obtained it is chosen that falling closer to a given condition which characterizes the family searched for. This solution indicates an area in the search parameters space where solutions of the kind

searched for might be found. Further and thinner scanning around the points selected in each parameters space sweep is used to improve the accuracy.

Since equations (3.18) constitute a second order system, in order to start the numerical method the values of the two unknown functions and its derivatives at some given transverse point need to be provided. Moreover to check the numerical procedure is working properly it is useful to monitor the values yielded for each harmonic's energy flow and the hamiltonian, whereupon the numerical function to obtain the vector of derivatives $\overrightarrow{y}$ in the numerical search, $f(\overrightarrow{y}, s) = d\overrightarrow{y}/ds$ is conveniently expressed

$$\begin{aligned}
y_{1_s} &= y_3, \\
y_{2_s} &= y_4, \\
y_{3_s} &= \tfrac{2}{r}\left(-\kappa_1 y_1 + y_1 y_2\right), \\
y_{4_s} &= \tfrac{2}{\alpha}\left(-\kappa_2 y_2 + y_1^2\right), \\
y_{5_s} &= y_1^2, \\
y_{6_s} &= y_2^2, \\
y_{7_s} &= -\tfrac{1}{2}\left(r y_3^2 + \tfrac{\alpha}{2} y_4^2\right) + \tfrac{\beta}{2} y_2^2 - y_1^2 y_{2.},
\end{aligned} \tag{3.27}$$

When searching for finite energy localized waves, minimum energy can be used as condition for solution selection, and concentrating on bright profiles a proper way of expressing the initial conditions is

$$\begin{aligned}
y_1 &= A_1, \\
y_2 &= A_2, \\
y_3 &= 0, \\
y_4 &= 0, \\
y_5 &= 0, \\
y_6 &= 0, \\
y_7 &= 0,
\end{aligned} \tag{3.28}$$

yielding a two dimensional parameters space $\{A_1, A_2\}$ left for shooting search.

Further simplification comes through manipulation of the stationary equations (3.18) using

$$\frac{\partial^2}{\partial s^2} = \frac{\partial U}{\partial s}\frac{\partial}{\partial U}\left(\frac{\partial U}{\partial s}\right)\frac{\partial}{\partial U} + \left(\frac{\partial U}{\partial s}\right)^2 \frac{\partial^2}{\partial U^2} = \frac{1}{2}\frac{\partial}{\partial U}\left(\left(\frac{\partial U}{\partial s}\right)^2\right)\frac{\partial}{\partial U} + \left(\frac{\partial U}{\partial s}\right)^2 \frac{\partial^2}{\partial U^2}, \tag{3.29}$$

and integrating in U_1 and U_2 respectively in each of the stationary equations. One obtains

$$\begin{aligned} \frac{r}{2}U_{1_s}^2 + \kappa_1 U_1^2 - 2\int U_1 U_2 dU_1 &= C_1, \\ \frac{\alpha}{4}U_{2_s}^2 + \frac{\kappa_2}{2}U_2^2 - \int U_1^2 dU_2 &= C_2, \end{aligned} \tag{3.30}$$

where C_1 and C_2 are integration constants. The integral terms in these equations can be resolved by adding them together whereupon a first integral of equations (3.18) is obtained which reads

$$\frac{r}{2}U_{1_s}^2 + \frac{\alpha}{4}U_{2_s}^2 + \kappa_1 U_1^2 + \frac{\kappa_2}{2}U_2^2 - U_1^2 U_2 = C, \tag{3.31}$$

with $C = C_1 + C_2$. For finite energy localized waves, vanishing fields at $s \longrightarrow \pm\infty$ require $C_1 = C_2 = 0$ hence it is set $C = 0$ which even though it does not disallow the possibility of $C_1 = -C_2$ with C_1, C_2 finite, it provides direct information about the solutions searched for.

The above relation can be used to reduce the dimensionality in the parameters space of the shooting method by providing a connection between the fields amplitudes at $s = 0$. Recalling that localized waves with a bright shape are searched for, let $U_{1_s}(0) = U_{2_s}(0) = 0$ in (3.31) to obtain

$$A_1^2 = \frac{\kappa_2 A_2^2}{2(A_2 - \kappa_1)}, \tag{3.32}$$

This expression can be regarded as the generalization of Kaplan's result [137], $U_2(0) = \kappa_1$, $U_2(0) = \sqrt{\kappa_1 \kappa_2}$ for the intensities of the plane-wave stationary states to finite, localized beams. For the present solitary wave solution search has the important implication of relating the two parameters in the shooting search so that the shooting is reduced to one dimension.

To ensure the occurrence of bright-shaped solutions one may simply examine the sign of $U_{1_{ss}}$ at $s = 0$ which is given by equations (3.18). Using the above relation one has for bright amplitude profiles

$$U_{1_{ss}}|_{s=0} = \frac{\kappa_2 A_2^2}{r A_1} < 0, \tag{3.33}$$

$$U_{1_{ss}}|_{s=0} = \frac{\kappa_2 A_2 (2\kappa_1 - A_2)}{\alpha (A_2 - \kappa_1)} < 0. \tag{3.34}$$

Without loss of generality, since the governing equations are invariant under changes of sign in U_1, let $A_1 > 0$. For given values of r and α, the signs of κ_1 and κ_2 are determined so to give

exponential decaying tails when $s \longrightarrow \pm\infty$. Basically $\kappa_1/r > 0$, $\kappa_2/\alpha > 0$ (see section 3.4). Therefore the signs of r and α and the value of A_2 determine the regions in parameters space where localized solutions with the simplest bright shape may exist.

Focusing in the spatial case ($r = -1$, $\alpha \simeq -0.5$), both nonlinear phase shifts are positive and by using (3.32) and (3.33-3.34), the search results greatly simplified through localization of A_2 between two bounds, namely

$$\kappa_1 < A_2 < 2\kappa_1, \tag{3.35}$$

Application of the shooting method to this problem simply consists on integration of the stationary equations by standard integration schemes such as for example Runge-Kutta, for different initial conditions obtained through systematic variation of the A_2 value between these two bounds. Throughout each scan the A_2 values that yield the lowest total energy are selected till enough accuracy is achieved that allows for a proper construction of the solution.

The analytic solution given by (3.23) provides an entry point which proves useful to start the numerical method and thus find the whole family of bright localized modes through small variations of the parameter κ_1.

This procedure has allowed obtention of the families of bright stationary field profiles, from which some illustrative examples are shown in Figure 3-2. In spite of a marked tendency to decay, after some distance from $s = 0$, the solutions feature ascending tails that can be attributed to instability of the numerical method when applied to solve equations (3.18). Confirmation of the nature of these ascending tails comes from application of the same method imposing initial conditions at infinity as it is discussed in section 3.4. This difficulty may as well be overcome by using a Newton-Raphson method, discussed in section 5.1.2 to solve the equations.

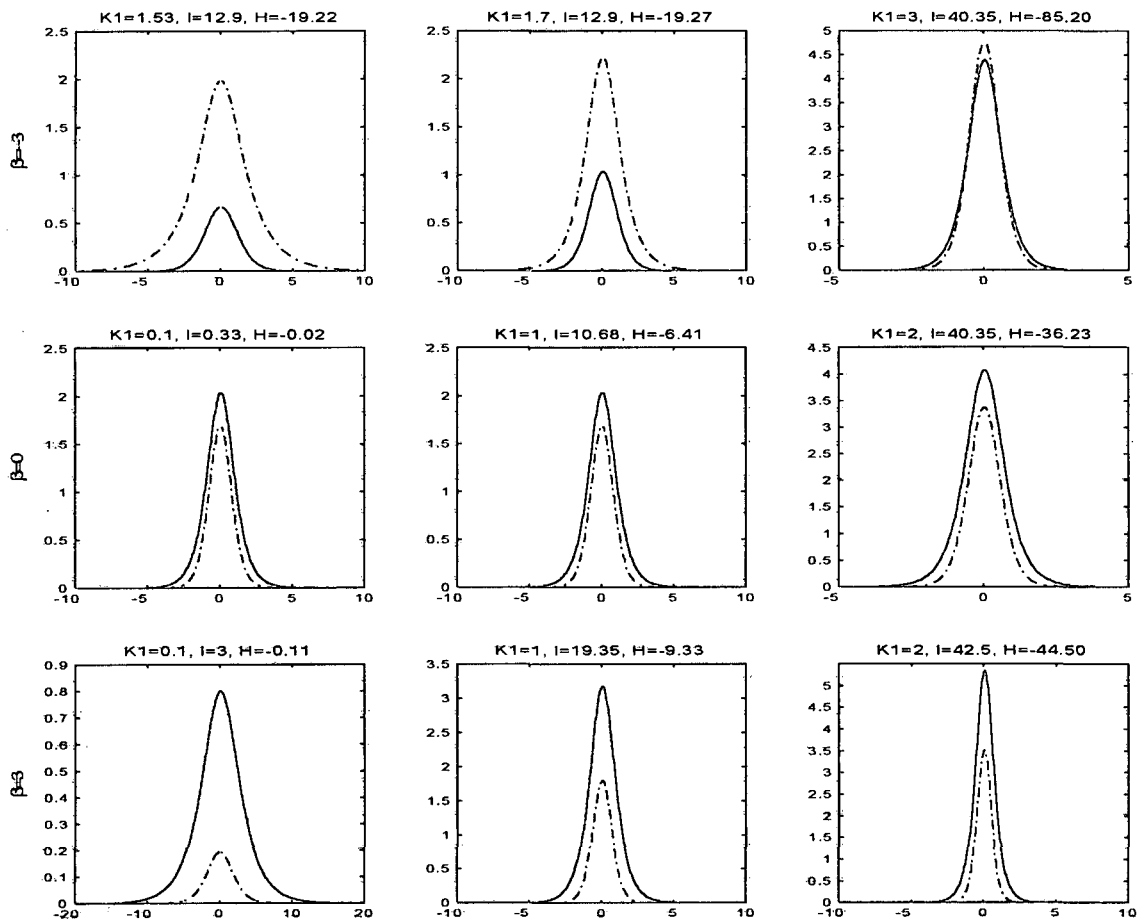

Figure 3-2: Some soliton transverse profiles for different values of the wavevector mismatch and the parameter γ_1. Red, continuous lines represent the FF while blue, dashed lines have been used for the SH.

3.2 Family of $(1+1)$ stationary bright solutions

This section is intended to constitute kind of a data base comprising all the basic characteristics of the solitary wave solutions in the best organized manner as possible so as to facilitate subsequent consultation for analysis and discussion or numerical experiments design.

When looking for a proper arrangement of data, one finds out that from the two parameters identified as defining the stationary solitary waves, β and κ_1, while the former is susceptible of being controlled by appropriate design of the $\chi^{(2)}$ sample, the latter is not. Since physically κ_1 represents a phase shift with a nonlinear origin, it depends on the total energy flow, I, which is a quantity that one does control by adjust of the total power injected into the waveguide. Hence, while from a mathematical point of view it is more convenient to use κ_1 as the parameter defining the family of solitons, when attending to physical aspects, the use of I is advised.

The relation between the search parameter κ_1 and the more physical parameter which will be used in the characterization of the solitary wave solutions, namely the total energy flow I, is presented in Figure 3-3 for negative, positive and zero phase mismatch values. Note that through application of the scaling rules enjoyed by the stationary equations (3.18), the same graphs may be obtained for any value of the phase mismatch starting from the three given. The loci where solitary waves are found in the $\mathcal{H}$-I plane, quite useful for graphical elucidation of stability of the solutions, is presented in Figure 3-3. Also in Figure 3-3 it is found the harmonics power sharing and peaks amplitude ratio plotted against total energy flow, the same characteristics which in Figure 3-4 are plotted against linear phase mismatch. Basically it is seen that as $|\beta|$ is increased, the second harmonic content is reduced for $\beta > 0$ and increased for $\beta < 0$. For exact phase matching both the peak amplitude relation and the power sharing between harmonics remains constant against total energy flow while for $\beta \neq 0$, since an increase in total energy flow nonlinearly reduces the effective wavevector mismatch, the soliton energy sharing between harmonics behaves accordingly.

Probably the most striking observation which arises from direct inspection of the plots is the fact that while for positive and zero wavevector mismatch configurations solitary waves may form with any total energy flow value, a threshold energy flow needs to be exceeded for solitary wave propagation to take place in negative wavevector mismatch configurations. As it will be

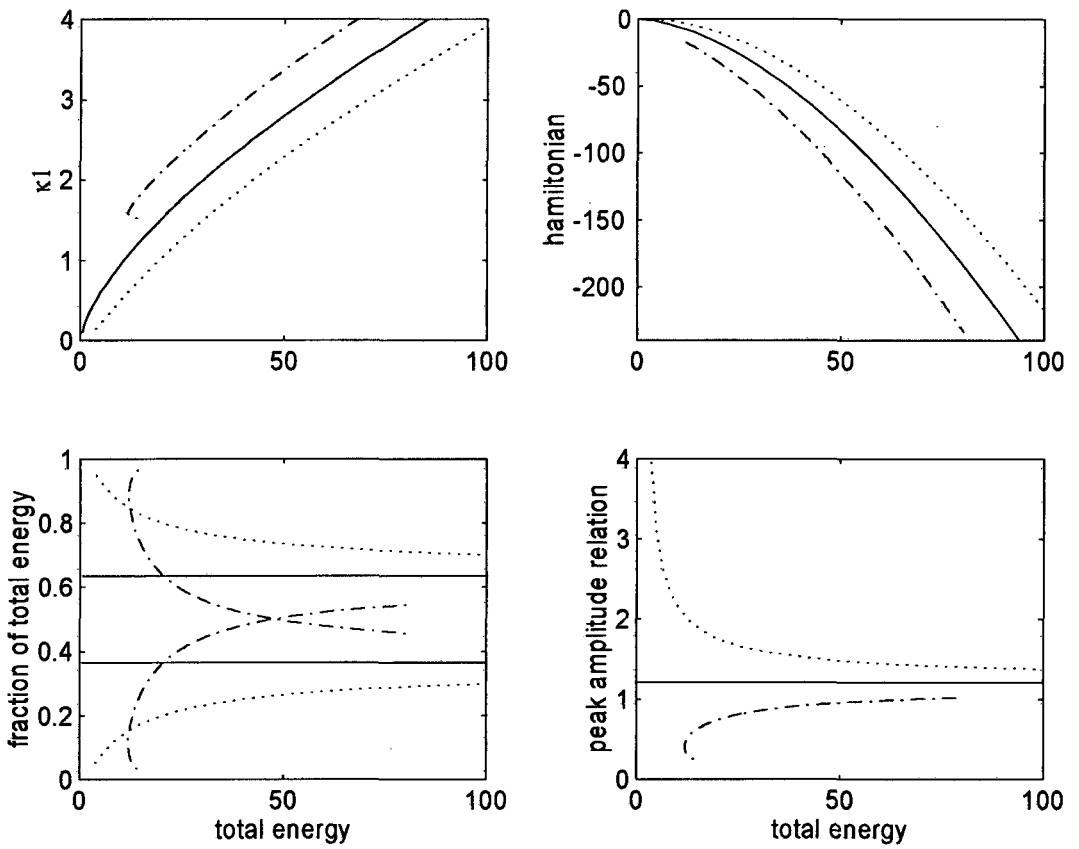

Figure 3-3: Some features of the solitary wave solutions against total energy. (-): $\beta = 0$, (-.): $\beta = -3$, (:): $\beta = 3$. Red curves refer to quantities related to the FF field while blue lines correspond to SH values.

seen through the analysis of the soliton tails in section 3.4, the cut-off value is given by

$$\overline{\kappa}_{1_{CUT-OFF}} = -\frac{\beta}{2}. \tag{3.36}$$

Finally, characterization of the fields shapes comes through Figure 3-5 where the dependence of the beam widths at $1/e^2$ is plotted against their respective amplitudes and against the total power contained in the solution. Because the solitons feature increasingly broader beams as the power is lowered, for a given input beams width and from a practical viewpoint, an input energy threshold for soliton formation does exist also for $\beta > 0$. Also it is observed in the plots of Figure 3-5 that for a range of reasonably high power levels the solitons width is almost kept constant. Specifically for the case of exact phase matching it can be shown that the solitons feature a constant amplitude$\times$ (width)^2 relation.

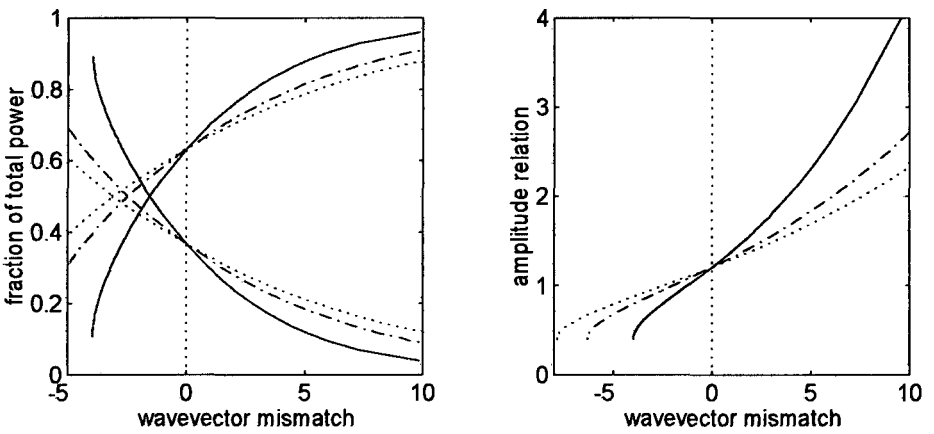

Figure 3-4: Power sharing between harmonics and A_1/A_2 amplitude relation plotted against wavevector mismatch (-): $I = 18$, (-.): $I = 36$, (:): $I = 50$. Red lines refer to the fundamental field while blue lines correspond to the second harmonic.

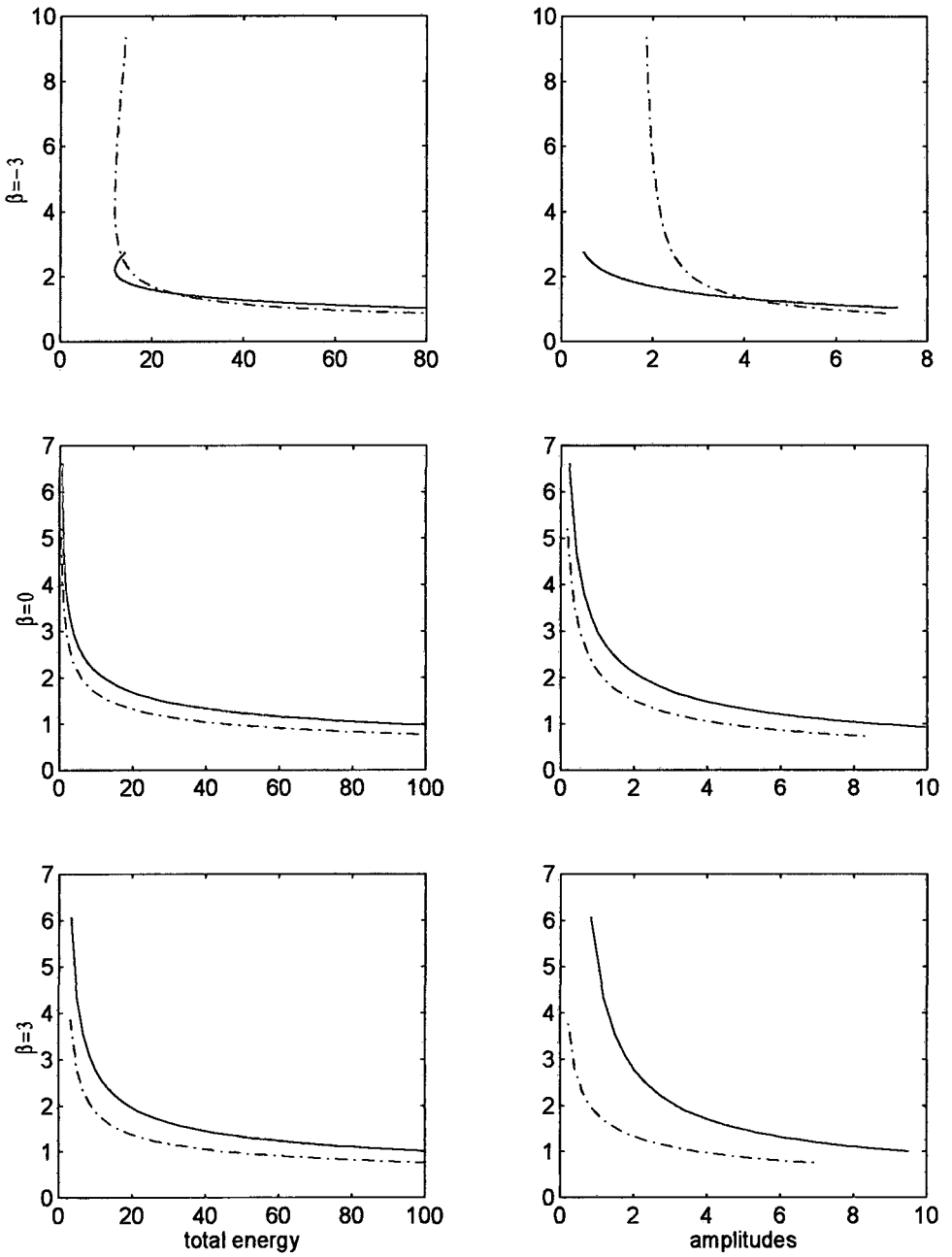

Figure 3-5: Widths of the solitary wave solutions plotted against total energy and the respective amplitudes for various values of the wavevector mismatch. (-) FF and (-.) SH.

3.3 Stability

The fact that the solitary wave solutions verify the stationary equations in (3.18) is not enough for claiming that solitary waves whose profiles follow those of the solutions will exist in the system. Such an assertion need to be supported by proofs of *stability*. Within the framework of the present analysis, stable solutions will be considered those which once reached by the system are maintained against small perturbations in the same number of transverse dimensions than the system where they have been found, meaning that modulational instabilities against higher-dimensional perturbations are not taken into account.

From the many approaches that can be used to elucidate the stability of a given family of solutions, see for example [71], the one providing a more direct graphical insight is the geometrical approach discussed right away.

3.3.1 Geometrical approach

In hamiltonian dynamical systems a connection may be established between the stability properties of a stationary solution and the value of its hamiltonian [139]-[140]. Specifically for the case analyzed here, generic stationary solutions with the form given by (3.1a) are shown to verify

$$\delta_F \left(\mathcal{H} + \kappa_1 I - v \mathcal{J} \right) = 0. \tag{3.37}$$

were δ_F stands for variational derivative.

In the case of the solitary waves existing in the absence of walk-off, one has

$$\mathcal{J} = -vI, \tag{3.38}$$

and the above is therefore written

$$\delta_F \left(\mathcal{H} + \overline{\kappa}_1 I \right) = 0. \tag{3.39}$$

Expression (3.37) as stating that stationary solutions with the form (3.1a) correspond to extrema of the hamiltonian for each pair of values of the total energy and the momentum, eases to a great extent elucidation of their stability. Only remains to resolve whether this extrema

consists of a minimum thus confirming the stability of the solutions or else if it is a maximum whereupon the solutions will be unstable.

Since no instability is shown when introducing in the numerical bpm input conditions whose hamiltonian values are close to that for the stationary solutions, but rather through evolution over long distances the input profiles seem to slowly tend to them (see Figures 3-8, 3-9), it is concluded that they realize a minimum of hamiltonian and hence are stable save for the upper branch of solutions found for close to threshold energy values in the negative β case. The progressive detachment from the input profiles shape towards something closer to the stationary profiles branch when these solutions are propagated using the numerical bpm is illustrated in Figure 3-7. That is one of the reasons conferring very limited physical relevance to the unstable solutions together with the fact that they feature increasingly broader beams and that in practice the input beams are not expected to match the exact shape of these solutions.

Actual calculation of the expression of the hamiltonian for solutions with the general form (3.1a) gives

$$\mathcal{H} = \int_{-\infty}^{\infty} \left(-\frac{r}{2} U_{1_s}^2 - \frac{\alpha}{4} U_{2_s}^2 + \frac{\beta}{2} U_2^2 - U_1^2 U_2 \cos(\Delta\psi) - \frac{\delta}{2} \phi_{2_s} U_2^2 \right) ds, \tag{3.40}$$

where $\Delta\psi = (2\kappa_1 - \kappa_2 + \beta)\,\xi + (2\mu_1 - \mu_2)\,s$.

Using integration by parts the first terms in this expression may written

$$\int_{-\infty}^{\infty} U_s U_s ds = U U_s|_{-\infty}^{\infty} - \int_{-\infty}^{\infty} U U_{ss} ds = -\int_{-\infty}^{\infty} U U_{ss} ds, \tag{3.41}$$

where it is made express use of the fact that derivatives should vanish at $|s| \longrightarrow \infty$ for localized structures. The above constitutes a very convenient way of putting these terms since it allows for substitution of U_{ss} using the governing equations thus providing an option for elimination of nonlinear terms in the hamiltonian.

For solutions with pure linear phase fronts recall that it was assumed (3.6) $\Delta\psi = 0$ which besides the phase locking condition, i.e. $\kappa_2 = 2\kappa_1 + \beta$, requires $2\mu_1 = \mu_2$ which in the spatial case is only possible when $\delta = 0$. The amplitude profiles on their side must verify equations (3.18) which yielded a first integral (3.31) relating the values of the first derivatives. Taking all

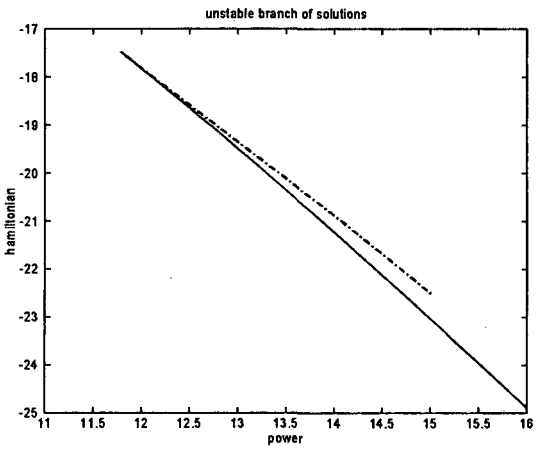

Figure 3-6: Zoom in the I-$\mathcal{H}$ plane to show the unstable branch of solutions(-.) found for $\beta = -3$ near the cutoff values.

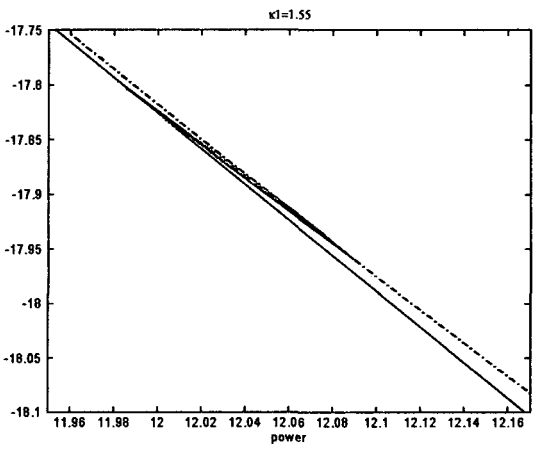

Figure 3-7: Example of evolution over the I-$\mathcal{H}$ plane of a solution of the unstable branch up to 500 normalized propagation distances.

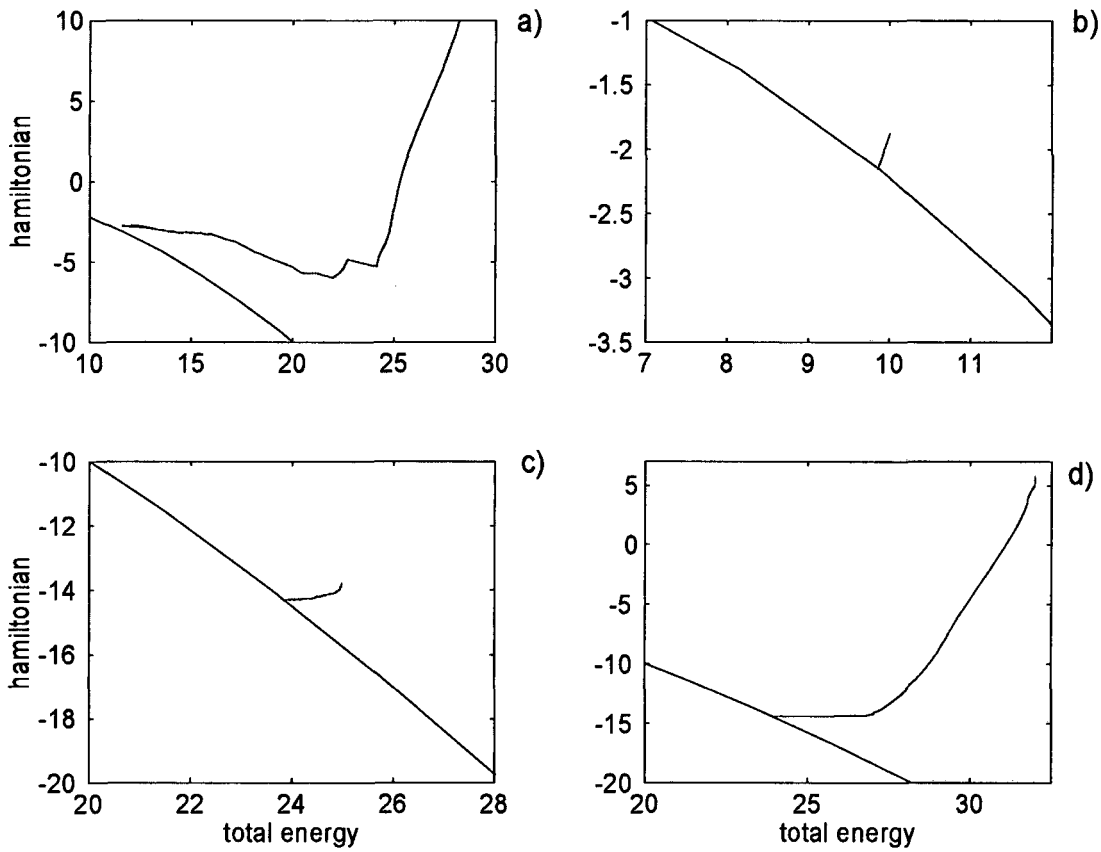

Figure 3-8: Examples of evolution over the I-$\mathcal{H}$ plane for $\beta = 3$. a) beam splitting occurring for $A_1 = 4$, $A_2 = 1$ and π relative phase. In b) and c) the amplitudes have been chosen to yield a minimum of $\mathcal{H}$ for $I = 10$, and $I = 25$ respectively. d) example of exclusive injection of the fundamental $A_1 = 4$. Normalized propagation distance $\xi = 500$.

this and (3.41) into account the hamiltonian is conveniently written

$$\mathcal{H} = \int_{-\infty}^{\infty} \begin{pmatrix} -\frac{4}{5}\frac{r}{2}U_{1_s}^2 - \frac{1}{5}\frac{r}{2}U_{1_s}^2 - \frac{4}{5}\frac{\alpha}{4}U_{2_s}^2 - \frac{1}{5}\frac{\alpha}{4}U_{2_s}^2 + \frac{\beta}{2}U_2^2 \\ -\frac{6}{5}U_1^2U_2 + \frac{1}{5}U_1^2U_2 \end{pmatrix} ds, \tag{3.42}$$

Substitution of selected terms using (3.41) combined with (2.94) and (3.31) leads to

$$\mathcal{H} = \int_{-\infty}^{\infty} \begin{pmatrix} \frac{4}{5}U_1\left(-\kappa_1 U_1 + U_1U_2\right) - \frac{r}{10}U_{1_s}^2 + \frac{2}{5}U_2\left(-\kappa_2 U_2 + U_1^2\right) - \frac{\alpha}{5}U_{2_s}^2 + \frac{\beta}{2}U_2^2 \\ -\frac{6}{5}U_1^2U_2 + \frac{1}{5}\left(\frac{r}{2}U_{1_s}^2 + \frac{\alpha}{4}U_{2_s}^2 + \kappa_1 U_1^2 + \frac{\kappa_2}{2}U_2^2\right) \end{pmatrix} ds, \tag{3.43}$$

finally arriving to the reduced expression

$$\mathcal{H} = -\frac{3}{5}\kappa_1 I_1 + \left(-\frac{3}{10}\kappa_2 + \frac{\beta}{2}\right) I_2, \tag{3.44}$$

which can be still further simplified by use of $2\kappa_1 = \kappa_2 - \beta$ and $I = I_1 + I_2$ to get a closed expression for the hamiltonian of stationary solutions

$$\mathcal{H} = -\frac{3}{5}\kappa_1 I + \frac{1}{5}\beta I_2, \tag{3.45}$$

which unfortunately does not give a direct dependence upon the total energy flow that may allow direct obtention of the I-$\mathcal{H}$ curves but is found quite useful to test occurrence of stationary solutions in the numerical beam propagation simulations.

3.4 Soliton tails

Since nonlinear effects are often related to occurrence of high intensities, in the profile tails where the fields amplitudes have decayed down to very small values and by analogy with the linear beam propagation case, it is usual to assume that the fields amplitudes transverse dependence approximately follows an exponential function. That is, when $|s| \longrightarrow \infty$ the fields amplitudes may be expressed

$$U_1 \sim B_1 \exp\left(-\Gamma_1 s\right), \tag{3.46}$$

$$U_2 \sim B_2 \exp\left(-\Gamma_2 s\right). \tag{3.47}$$

That approximation actually steams from neglecting nonlinear terms in (2.94). Hence the assumption for the transverse fields dependence at $|s| \longrightarrow \infty$ formally is written

$$|a_1^* a_2| << |a_1| \longrightarrow U_2 << 1, \tag{3.48}$$

$$|a_1^2| << |a_2| \longrightarrow \frac{U_1^2}{U_2} << 1. \tag{3.49}$$

It is important to note that for the above approximation (3.49) to hold the constants of the assumed exponential decay in tails must verify

$$\Gamma_2 < 2\Gamma_1, \tag{3.50}$$

Now substitute the general expression for the travelling wave solutions (3.1a) into the linearized governing equations, i.e.

$$\begin{aligned} j a_{1_\xi} - \frac{r}{2} a_{1_{ss}} &= 0, \\ j a_{2_\xi} - \frac{\alpha}{2} a_{2_{ss}} - j\delta a_{2_s} &= 0, \end{aligned} \tag{3.51}$$

and separate real and imaginary part to get for the imaginary

$$\left(v + r\phi_{1_s}\right) U_{1_s} + \frac{r}{2} \phi_{1_{ss}} U_1 = 0, \tag{3.52}$$

$$\left(v + \delta + \alpha\phi_{2_s}\right) U_{2_s} + \frac{\alpha}{2} \phi_{2_{ss}} U_2 = 0. \tag{3.53}$$

At this point the assumption is made that the behavior in tails is such that the fields phase front can be approximated as a mere tilt whereupon $\phi_{1_{ss}} \underset{s\to\infty}{\longrightarrow} 0$, $\phi_{2_{ss}} \underset{s\to\infty}{\longrightarrow} 0$ and using the above

$$\phi_{1_s} \underset{s\to\infty}{\longrightarrow} -\frac{v}{r}, \tag{3.54}$$

$$\phi_{2_s} \underset{s\to\infty}{\longrightarrow} -\frac{(v+\delta)}{\alpha}. \tag{3.55}$$

If the harmonics don't exchange energy in the stationary state, the above equalities must

be such that they verify $\phi_{2_s} = 2\phi_{1_s}$, which is to say

$$\delta = \left(2\frac{\alpha}{r} - 1\right) v, \tag{3.56}$$

reminiscent of the result in (3.10) for stationary solutions with a pure phase front tilt.

For the solitary waves here analyzed ($r = -1$, $\alpha = -1/2$, $\delta = 0$), (3.54-3.55) reduce to

$$\phi_{1_s} \underset{s\to\infty}{\longrightarrow} v, \tag{3.57}$$

$$\phi_{2_s} \underset{s\to\infty}{\longrightarrow} 2v. \tag{3.58}$$

Real part of equations (3.51) gives

$$-\frac{r}{2}U_{1_{ss}} + \left(-\kappa_1 + v\phi_{1_s} + \frac{r}{2}\left(\phi_{1_s}\right)^2\right) U_1 = 0, \tag{3.59}$$

$$-\frac{\alpha}{2}U_{2_{ss}} + \left(-\kappa_2 + (v+\delta)\,\phi_{2_s} + \frac{\alpha}{2}\left(\phi_{2_s}\right)^2\right) U_2 = 0. \tag{3.60}$$

Assume exponential decaying tails as in (3.46) (3.47) and get

$$-\frac{r}{2}\Gamma_1^2 - \kappa_1 + v\phi_{1_s} + \frac{r}{2}\left(\phi_{1_s}\right)^2 = 0, \tag{3.61}$$

$$-\frac{\alpha}{2}\Gamma_2^2 - \kappa_2 + (v+\delta)\,\phi_{2_s} + \frac{\alpha}{2}\left(\phi_{2_s}\right)^2 = 0, \tag{3.62}$$

which through substitution of the previous result (3.54) (3.55) yields for the exponential decay constants

$$\Gamma_1^2 = -\frac{2}{r}\kappa_1 - \frac{v^2}{r^2}, \tag{3.63}$$

$$\Gamma_2^2 = -\frac{2}{\alpha}\kappa_2 - \frac{(v+\delta)^2}{\alpha^2}. \tag{3.64}$$

For the specific case of stationary solutions with purely linear phase fronts recall the nonlinear phase shifts redefinitions (see (3.12)) to write for the spatial beam propagation case ($\alpha = -0.5$, $r = -1$) the following

$$\Gamma_1^2 = 2\overline{\kappa}_1 + v^2, \tag{3.65}$$

$$\Gamma_2^2 = 4\left(\overline{\kappa}_2 + v^2\right) = 4\left(2\overline{\kappa}_1 + \beta + v^2\right), \tag{3.66}$$

where express use has been made of the fact that in the spatial case it must be $\delta = 0$. A result that is consistent with the assumptions made to obtain it (3.50) only if $\beta < 0$.

Assuming soliton traveling in the straight direction, $v = 0$, real values for the exponential decay constants in tails, Γ_1 and Γ_2, require

$$\overline{\kappa}_1 > 0 \ , \ \overline{\kappa}_1 > -\frac{\beta}{2}, \tag{3.67}$$

thus determining the cut-off value for negative β solitons to exist as

$$\overline{\kappa}_{1_{CUT-OFF}} = -\frac{\beta}{2}. \tag{3.68}$$

The fact that expressions (3.66-3.66) are not consistent with the linear approximation in tails leads to the conclusion that the fields decay in the case of $\beta > 0$ either is not purely exponential as assumed in (3.46-3.47) or else that there is a contribution of nonlinear terms in equations (3.51) that hence violates the assumption in (3.49). The answer is found through inclusion into the derivation of the previously neglected nonlinear term in the equation for the second harmonic.

Since total absence of local energy exchange between harmonics is assumed, i.e. $\phi_2 = 2\phi_1$, the nonlinear term to include only affects the equation for the real part, hence copying from (3.60) one has

$$-\frac{\alpha}{2}U_{2_{ss}} + \left(-\kappa_2 + (v+\delta)\,\phi_{2_s} + \frac{\alpha}{2}\left(\phi_{2_s}\right)^2\right)U_2 = -B_1^2 \exp\left(-2\Gamma_1 s\right), \tag{3.69}$$

where based on fulfillment of (3.48) the exponential decay approximation is assumed to be valid for the fundamental profile which hence acts as a forcing term for the second harmonic transverse dependence in tails.

Now applying the result in (3.55) one gets

$$U_{2_{ss}} + \frac{2}{\alpha}\left(\kappa_2 + \frac{(v+\delta)^2}{2\alpha}\right)U_2 = \frac{2}{\alpha}B_1^2 \exp\left(-2\Gamma_1 s\right), \tag{3.70}$$

which is readily solved to give for the second harmonic soliton tails

$$U_2 \sim B_2 \exp\left(-\Gamma_2 s\right) + \frac{2}{\alpha} \frac{B_1^2}{4\Gamma_1^2 - \Gamma_2^2} \exp\left(-2\Gamma_1 s\right), \tag{3.71}$$

where Γ_1 and Γ_2 are given by expressions (3.63), (3.64) respectively which in the spatial case lead to

$$U_2 \sim B_2 \exp\left(-\Gamma_2 s\right) + \frac{B_1^2}{\beta - 2\delta v - \delta^2} \exp\left(-2\Gamma_1 s\right), \tag{3.72}$$

giving for purely tilted soliton solutions setting $\delta = 0$,

$$U_2 \sim B_2 \exp\left(-\Gamma_2 s\right) + \frac{B_1^2}{\beta} \exp\left(-2\Gamma_1 s\right), \tag{3.73}$$

Since as it has been verified numerically, as $\beta \longrightarrow \infty$, $\exp\left(-\Gamma_2 s\right) \sim \exp\left(-\sqrt{\beta} s\right) \longrightarrow 0$ far more quickly than $B_2 \longrightarrow -\infty$, the first of the terms in this expression goes to zero for very large β, which is perfectly consistent with the result in the NLSE limit namely

$$a_2 = \frac{a_1^2}{\beta}. \tag{3.74}$$

For $\beta = 0$ one has $\Gamma_2 = 2\Gamma_1$, and from equation (3.70) it is obtained

$$U_2(|s| \longrightarrow \infty) = \left(B_2 + \frac{B_1^2}{\Gamma_1} s\right) \exp\left(-2\Gamma_1 s\right) \tag{3.75}$$

Expression (3.73) constitutes actually an extension of (3.47) for the case of positive β since it contains the two possible β signs, namely

$$\beta < 0 \longrightarrow \Gamma_2 < 2\Gamma_1 \longrightarrow U_2(|s| \longrightarrow \infty) = B_2 \exp\left(-\Gamma_2 s\right), \tag{3.76}$$

$$\beta > 0 \longrightarrow \Gamma_2 > 2\Gamma_1 \longrightarrow U_2(|s| \longrightarrow \infty) = \frac{B_1^2}{\beta} \exp\left(-2\Gamma_1 s\right), \tag{3.77}$$

$$U_1(|s| \longrightarrow \infty) = B_1 \exp\left(-\Gamma_1 s\right) \text{ for all } \beta \text{ values.} \tag{3.78}$$

Concerning fulfillment of $\Delta\phi = 0$ stability requirement one has that in the soliton tails

$$\Delta\phi = \frac{U_{1ss}}{U_1} - \frac{1}{4}\frac{U_{2ss}}{U_2} - |\beta|, \beta < 0, \tag{3.79}$$

$$\Delta\phi = -\frac{B_1^2}{B_2} + |\beta| \ , \beta > 0 \ . \tag{3.80}$$

Note that while linear diffraction terms are cancelled at $|s| \longrightarrow \infty$ in the positive β case so that maintenance of phase locking condition is achieved through the action of nonlinear terms which ensure it through the amplitude values; it is nonlinear terms which go to zero in the negative β case whereupon the phase locking condition has to rely upon linear diffraction terms and therefore upon the transverse profile dependence.

A striking feature revealed by this analysis is that unlike typical soliton propagation problems, in the case of positive β nonlinear terms contribute to the fulfillment of $\Delta\phi = 0$ condition in tails so that basically, at $|s| \longrightarrow \infty$,

$$\frac{B_1^2}{B_2} = \beta. \tag{3.81}$$

Agreement is found between the transverse dependences in tails showed by the stationary solutions numerically found through the shooting and the above derivation. Furthermore, by properly fitting exponentials to the tails of these numeric solutions one can actually calculate to some degree of accuracy the values of the constants in expressions (3.76-3.78), Figures 3-10, 3-11.

Starting from the transverse dependences in tails just derived and by giving values to the parameter κ_1 which through freezing the transverse functional profiles dependence at $|s| \longrightarrow \infty$ acts as the parameter defining the families of stationary solutions existing for each value of β, the whole transverse dependence of the stationary solutions possible for any value of κ_1 may be obtained through the use of standard numerical integration starting from $|s| \longrightarrow \infty$ and evolving towards the center provided the proper amplitude values at infinity B_1 and B_2 are chosen so that a transverse curve closed into itself is obtained yielding bounded energy. That entails solving a complicated two dimensional shooting problem since no clues on the approximate region in the two dimensional space where the solutions might be found are easily derived. However by taking the results in Figures 3-10, 3-11 as a guess one can, starting the numerical integration from $s = \infty$, actually obtain the same curves than when the numerical method is started from $s = 0$ thus confirming the nature of eventual ascending tails as coming from instabilities of the method used to integrate the equations and being not a characteristic of the solutions.

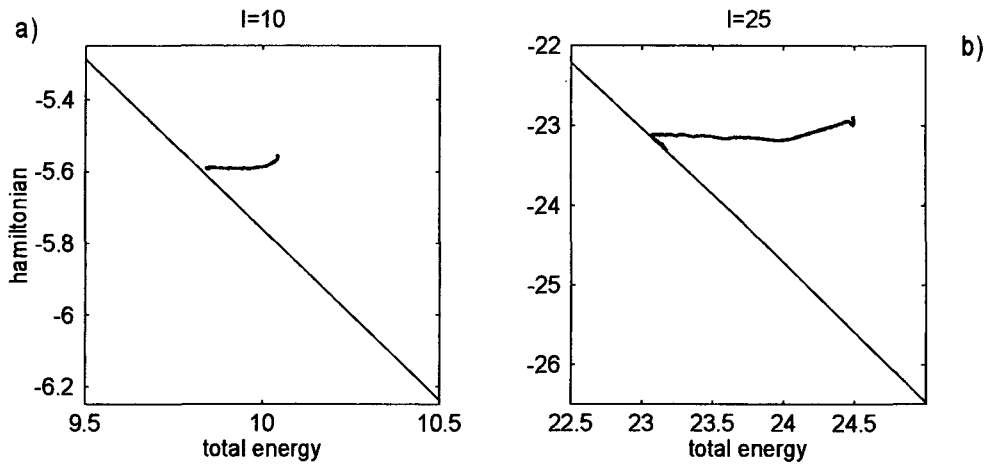

Figure 3-9: Examples of evolution over the I-$\mathcal{H}$ plane for $\beta = 0$. The amplitudes have been chosen to yield a minimum of $\mathcal{H}$ for a) $I = 10$ and b) $I = 24.5$. Normalized propagation distance $\xi = 500$.

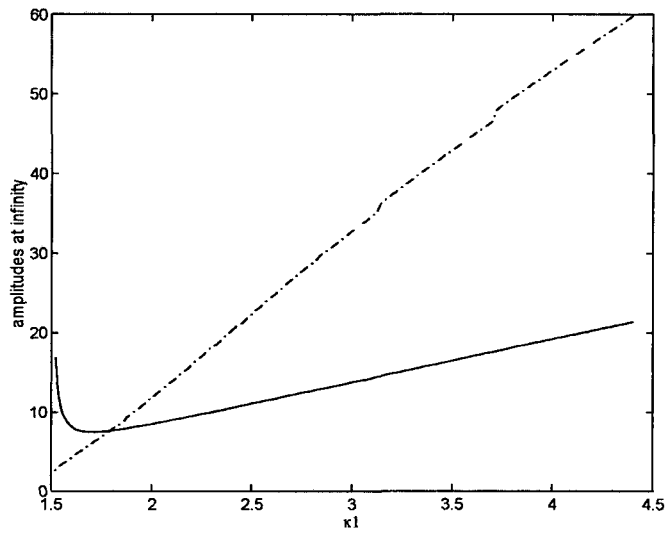

Figure 3-10: Amplitudes B_1 (-) and B_2 (-.) giving the transverse exponential dependence in the decaying profile tails for $\beta = -3$ as a function of the fundamental nonlinear wavevector κ_1.

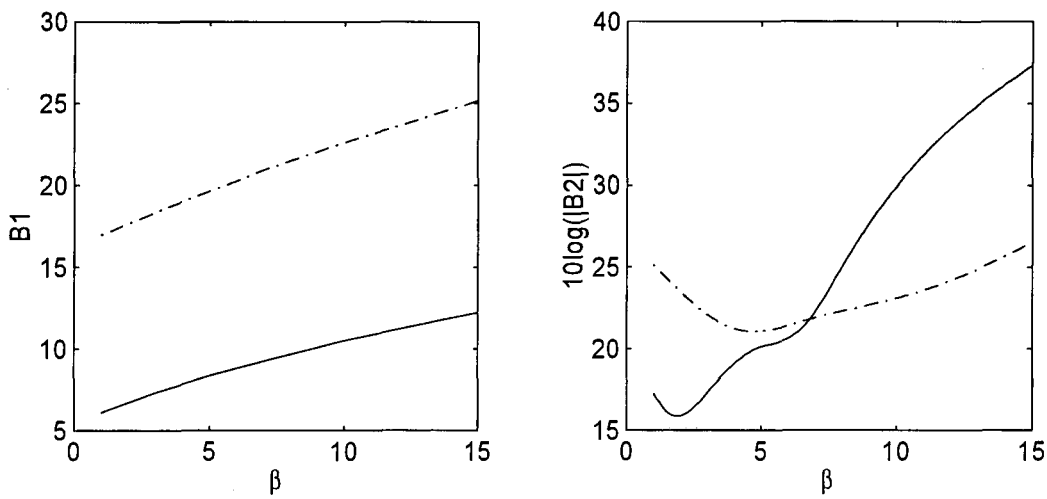

Figure 3-11: Wavevector mismatch dependence of the amplitudes defining the decaying dependence of the transverse profiles for positive β. (-): $\kappa_1 = 1$, (-.): $\kappa_1 = 3$.

3.5 Intuitive view of soliton solutions characteristics

At this point it is worth stopping for a while and try to develop an intuitive model that can help to understand the features displayed by the stationary solutions and how they preserve their shape on propagation. All conclusions obtained from this intuitive analysis will be shown to be consistent with the results in section 3.2 for the numerically found bright stationary solutions.

3.5.1 Generalities

Shape preservation on propagation for the stationary solitary waves can be understood from the point of view that each transverse profile point of each harmonic should maintain its 'local' energy on propagation. Formally that implies that the ξ derivatives in (2.113), (2.114) should be kept equal to zero while physically it means that neither energy exchange between harmonics nor energy dragging between transverse points should take place or else that a proper equilibrium is reached between both forms of energy exchange so that the profiles shape is maintained on propagation. Recall that the former was assumed to be the case for obtention of the solitary waves that exist in the absence of walk-off and hence is taken as the basis where the present intuitive analysis relies on.

The requirement for no energy exchange between harmonics is connected to fulfillment and keeping along propagation of the nonlinear phase matching condition which comprises both the $\Delta\psi = 0$ and $\Delta\psi_\xi = 0$ requirements, namely

$$\Delta\psi = 2\psi_1 - \psi_2 + \beta\xi = 0, \tag{3.82}$$

and

$$\Delta\psi_\xi = 2\psi_{1_\xi} - \psi_{2_\xi} + \beta = 0, \tag{3.83}$$

Using the expressions in (2.119), (2.120) one has

$$\Delta\psi_\xi = -r\frac{U_{1ss}}{U_1} + \frac{\alpha}{2}\frac{U_{2ss}}{U_2} + r\left(\psi_{1_s}\right)^2 - \frac{\alpha}{2}\left(\psi_{2_s}\right)^2 - \delta\psi_{2_s} + 2U_2\cos\left(\Delta\psi\right) - \frac{U_1^2}{U_2}\cos\left(\Delta\psi\right) + \beta = 0. \tag{3.84}$$

In addition to that, for solitary wave propagation along the planar waveguide to be possible, the nonlinear parametric interaction must compensate linear diffraction to yield a constant

wavefront for both harmonics.

Letting

$$\psi_{1,2} = \mu_{1,2} s + \kappa_{1,2} \xi, \tag{3.85}$$

the linear tilts μ_1 and μ_2 correspond to stationary waves propagating at an angle with respect to the z axis and κ_1 and κ_2 are the nonlinear phase constants for each harmonic. In order to avoid energy exchanges between harmonics, in the stationary state these constants must verify

$$\mu_2 = 2\mu_1, \tag{3.86}$$

$$2\kappa_1 - \kappa_2 + \beta = 0, \tag{3.87}$$

the latter already identified as the phase locking condition for nonlinear adjustment of the harmonic's propagation constants. Using that, and as derived, $\delta = 0$, (3.84) yields

$$\Delta\psi_\xi = -r\frac{U_{1ss}}{U_1} + \frac{\alpha}{2}\frac{U_{2ss}}{U_2} + 2U_2 \cos(\Delta\psi) - \frac{U_1^2}{U_2}\cos(\Delta\psi) + \beta = 0. \tag{3.88}$$

Through substitution of (3.85) into the expressions for the phases evolution it is obtained

$$\kappa_1 + \frac{\mu_1^2}{2} = \frac{1}{2}\frac{U_{1ss}}{U_1} + U_2 \cos(\Delta\psi), \tag{3.89}$$

$$\kappa_2 + \frac{\mu_2^2}{4} = \frac{1}{4}\frac{U_{2ss}}{U_2} + \frac{U_1^2}{U_2}\cos(\Delta\psi), \tag{3.90}$$

which gives a clear illustration on how linear diffraction represented by the first terms on the right hand side should on each harmonic be counteracted by the corresponding parametric interaction with the other harmonic accounted for in lasts terms on the right hand side, to yield a constant left hand side and hence purely tilted phase fronts for the solitary wave solutions. Expressions (3.89), (3.90) provide another possible lecture of the nonlinear phase matching or $\Delta\psi = 0$ condition for stationary solutions as ensuring maximum efficiency of the parametric interaction to compensate the effect of linear diffraction.

3.5.2 Nonlinear phase matching and interharmonics energy exchange

Starting with analysis of the first of the requirements derived for stationary solutions, namely absence of energy exchange between the harmonics, the nonlinear phase matching, i.e. $\Delta\psi = 0$, and its maintenance, i.e. $\Delta\psi_\xi = 0$, in every transverse point, may as well be understood as an equilibrium between energy exchanges of either direction for either sign of $\Delta\psi$ where the parameter β plays a key role as it shall be seen.

Deviations of $\Delta\psi$ from its stationary value are compensated through the energy exchange processes in such a way that when $\Delta\psi_\xi > 0$, energy flow which as dictated by (2.113), (2.114) is from second harmonic to fundamental, causes the fourth term in (3.88), i.e. $\frac{U_1^2}{U_2}\cos(\Delta\psi)$, to grow to the detriment to the third, $U_2\cos(\Delta\psi)$ whereupon $\Delta\psi_\xi$ reverses its sign. The dual situation is produced when $\Delta\psi_\xi > 0$, so that the deviation is recovered as well.

About the role played by β in the keeping of the nonlinear phase matching, one may say that it states a constant monotonic tendency for $\Delta\psi$ that has to be compensated by the rest of the terms in (3.88) thus determining their stationary values. From these terms, at the profiles peak the most important are third and fourth, hereafter referred to as nonlinear or amplitudes terms, because are susceptible of undergoing quick variations through the local energy exchange. Thus for positive β the contribution of these terms should be negative whereupon the peak amplitude relation verifies $A_1/A_2 > 1$, getting bigger for bigger β values. Using the same argument it must be $A_1/A_2 < 1$ and getting smaller for bigger $|\beta|$, for negative β.

On the other side, large peak values as accelerating the energy exchange process (recall that as seen from (2.113), (2.114) the energy exchange rate at a given transverse point is proportional to the $U_1^2U_2$ value in that point) relieve the requirements for compensation of the monotonic tendency imposed by β to $\Delta\psi$. Large peak local energy values are directly related to large energy flow I, hence, for the stationary solutions for positive β the A_1/A_2 amplitude relation decreases as the energy flow increases while the opposite occurs for negative β solitons.

As summary,

$$|\beta| \uparrow \longrightarrow U_1/U_2|_{STAT} \uparrow \longrightarrow I_1/I_2|_{STAT} \uparrow \quad \beta > 0$$

$$|\beta| \uparrow \longrightarrow U_1/U_2|_{STAT} \downarrow \longrightarrow I_1/I_2|_{STAT} \downarrow \quad \beta < 0$$

$$I \uparrow \longrightarrow U_1/U_2|_{STAT} \downarrow \longrightarrow I_1/I_2|_{STAT} \downarrow \ \beta > 0$$

$$I \uparrow \longrightarrow U_1/U_2|_{STAT} \uparrow \longrightarrow I_1/I_2|_{STAT} \uparrow \ \beta < 0$$

3.5.3 Energy dragging equilibrium

Although the condition for maintenance of the nonlinear phase matching, i.e. $\Delta\psi = 0$, has proven useful in describing the dependences for the 'peak' amplitudes ratio, complete stability of a given stationary solution is not totally guaranteed unless its transverse profile dependence ensures that eventual energy dragging exchanges between neighboring transverse points are successfully counteracted before variations of transverse local energy altering the energy exchange velocities and therefore the requirement on amplitudes ratio for equilibrium, lead to a succession of energy exchanges that break stationarity. Based on this idea what can be called *energy dragging stability requirement* is built up. The condition derived will be shown useful to intuitively understand the transverse profiles dependence of the stationary solutions.

For proper keeping of energy dragging equilibrium, the stationary transverse profile dependence must guarantee that eventual phase front variations causing differential energy dragging among transverse points of the profile and therefore altering the amplitudes relations, will be counteracted through enough change in linear diffraction terms so that both terms at the right hand side of expressions (3.89-3.90) mutually cancel respective variations.

Consider for example that a certain transverse point of a solitary wave profile experiences a sudden decrease of either of its nonlinear phase constants while its neighboring transverse points keep theirs. The mechanism of energy dragging will drag local energy out of the transverse point and deliver it to its neighbors in such a way that while the interharmonics energy exchange into the transverse point under consideration is slowed down, its neighbors exchange energy between harmonics still faster. That will cause differences in nonlinear phase matching values that will translate through the last term in right hand side of expressions (3.89-3.90) in enhanced phase differences that favour more energy dragging exchange. For the equilibrium to be restored before it is too late and the energy exchange disequilibrium drives the system too far away from solitary wave propagation, the only hope is that the harmonics transverse distribution is such that any punctual energy loss into any transverse point causes an increase of the its linear diffraction term (U_{ss}/U) that quickly enough compensates the sudden nonlinear phase front

drop.

Hence, just in the same way that a proper balance between amplitude values is required to compensate on time slight deviations that otherwise could grow due to interharmonics energy exchange till totally destroying the soliton or evolving into another solution, a proper transverse distribution is crucial to prevent slight destabilizations from causing severe damage in the solitary wave solution through growing action of energy dragging followed by interharmonics energy exchange.

Since an increase of local energy entails an acceleration of the interharmonics energy exchange process, for the sake of a quicker reaction against eventual nonlinear phase front variations that alter the energy content in each transverse point and hence its interharmonics energy exchange velocity, sharper profiles are required when the total energy flow associated with a given solitary wave solution increases. Likewise, higher phase mismatch absolute values as further reducing the effectiveness of the nonlinear parametric interaction for mismatched amplitude values yield smoother profiles. Schematically

$$|\beta| \uparrow \longrightarrow \text{ smoother profiles}$$

$$I \uparrow \longrightarrow \text{ sharper profiles}$$

As a summary of this intuitive view of the stationary solutions characteristics, one may conclude that while the nonlinear phase matching condition establishes the stationary harmonics peak amplitude relation in such a way that the energy exchange processes at each side of $\Delta\psi = 0$ condition are balanced so as to compensate any deviation from the stationary amplitude values, the energy dragging stability requirement determines the transverse profiles shape around center that ensures through change in linear diffraction terms, proper compensation of slight energy dragging exchanges among neighboring transverse points.

3.5.4 About the behavior in the soliton tails

While as for the analysis of peak amplitudes dependence the cases of $\beta > 0$ and $\beta < 0$ present analogous features, is in the transverse profiles dependence where the greatest differences are found.

Probably the most striking one is the existence of a threshold energy flow below which no stationary solutions are found for the $\beta < 0$ case whereas in the $\beta > 0$ case stationary solutions are possible for any total power. The threshold is viewed from the analysis of the transverse dependence in tails as the lower κ_1 value for which the constant of exponential decay of the second harmonic profile which as derived is obtained as $\Gamma_2 = \sqrt{2\kappa_1 + \beta}$, yields real values. Nonlinear phase matching achieved through adjustment of the harmonics amplitude relation in tails and always verifying $\Gamma_2 = 2\Gamma_1 = 2\sqrt{\kappa_1}$ explains absence of energy threshold for the existence of solitary wave solutions in the positive β case.

No solutions can be formed in the case of negative β relying on nonlinear or amplitudes terms for nonlinear phase matching in tails since the term opposing the sign of β in the $\Delta\psi$ expression (3.88) is $2U_2$ which unavoidably tends to zero at $|s| \longrightarrow \infty$ for bounded solutions.

Conversely, for positive β, the nonlinear phase matching cannot be achieved through the action of linear diffraction terms since that would mean $\Gamma_2 > 2\Gamma_1$ whereupon the nonlinear term U_1^2/U_2 would unboundedly exponentially increase as $|s| \longrightarrow \infty$. On the other side though, the sign of this nonlinear term as opposing that of β allows for achieving the nonlinear phase matching in tails through adjustment of the harmonics decreasing velocities as $|s| \longrightarrow \infty$ so that $U_1^2/U_2 \longrightarrow \beta$.

As for other differences between the transverse profiles for positive and negative phase mismatch bright stationary solutions, in few words it can be said that while for the $\beta > 0$ case the harmonics relative transverse dependencs in tails is fixed so that the second harmonic leading exponential dependence is the square of that for the fundamental for any value of the parameter κ_1, in the $\beta < 0$ case this harmonics relative transverse dependence has to be adapted to fulfil $\Delta\psi = 0$ condition in tails going from $\Gamma_1/\Gamma_2 >> 1$ for low κ_1 values up to $\Gamma_1/\Gamma_2 < 1$ for high ones. The latter is always the case for positive β whereupon all the stationary solutions are stable whereas in the negative β case as approaching threshold unstable solutions are found.

The instability can be intuitively understood by considering the nonlinear phase constant expression a differential step away from $|s| = \infty$ where the exponential behavior starts to deviate from the pure exponential,

$$\kappa_1 = \frac{1}{2}\Gamma_{1_{EFF}}^2 + U_2, \tag{3.91}$$

$$\kappa_2 = \frac{1}{4}\Gamma_{2_{EFF}}^2 + \frac{U_1^2}{U_2}, \tag{3.92}$$

where it has been assumed nonlinear phase matching. The parameters $\Gamma_{1_{EFF}}$ and $\Gamma_{2_{EFF}}$ denote the slightly different decay exponents found a differential step away from $|s| = \infty$ as required to vary following the amplitudes evolution for the sake of maintenance of the nonlinear phase constant values, κ_1 and κ_2. Hence, the amplitudes terms at the right hand side of expressions (3.91-3.92) at $|s| \longrightarrow \infty$ are referred to as *decay exponents correction factors* and read

$$CF_1 = B_2 \exp\left(-\Gamma_2 s\right), \tag{3.93}$$

$$CF_2 = \frac{B_1^2}{B_2} \exp\left(-\left(2\Gamma_1 - \Gamma_2\right) s\right). \tag{3.94}$$

These correction factors determine the progressive decrease in decay exponents required as approaching center in the numerical integration from $|s| = \infty$ for the amplitude profile curves to close into themselves yielding bounded energy. If the correction factors do not significantly increase as evolving towards the center, the amplitude profile will keep on increasing at the exponential rate. Attending at the correction factors amplitude dependence, this is specially worrying when at $|s| \longrightarrow \infty$ one has $CF_1 >> CF_2$ (which entails $\Gamma_2 << \Gamma_1$) meaning that while the fundamental soon loses its exponential dependence and hence increases slowly as approaching $s = 0$, the second harmonic amplitude is undergoing a fast (exponential) increase. This swift second harmonic amplitude grow is in turn hindering $CF_2 = U_1^2/U_2$ increase, further reducing the options for stopping the second harmonic fast increase. When both Γ_1 and Γ_2 are low one has on one side that CF_1 in $|s| = \infty$ is higher resulting in slower fundamental amplitude increase as approaching $s = 0$, whereupon the second harmonic amplitude curve bending down point must fall closer to the center; and on the other that the second harmonic amplitude evolution towards the center is slower. These two effects contribute to increase the area below the U_2 curve which results in nonlinear phase matching in peak achieved with a too broad transverse profile. The effect is more critical when the difference between decay exponents is larger, i.e. as $|\beta|$ increases, yielding larger values for the energy flow threshold to be exceeded to excite an stable soliton solution.

These too broad solutions hence evolve into unbalanced oscillating states in which during the focusing periods the profiles peak experiences a great increase of its local energy before

linear diffraction terms can contribute with the energy exchange to restore the equilibrium. The profiles peak may then else recover nonlinear phase matching soon enough as to absorb the increase in local energy so that through successive focusing and defocusing periods it progressively achieves the nonlinear phase matching with higher peak local energy values the profiles becoming sharper, usually tending to reshape into a solution of the stable branch, or else fail to restore the equilibrium on time whereupon the locking will take place around progressively lower peak local energy values eventually leading to the soliton destruction or break-up.

3.6 Exploring the dynamical regime

3.6.1 Monitoring the evolution: $I - \mathcal{H}$ planes and Stokes parameters

In laboratory setups, generally, no exact control upon the light beam characteristics can easily be performed and therefore there is little one can do to adapt the output of its light source to given requirements. There relies the great importance given to the study of the dynamics of the evolution towards an stationary state. For the solitary wave solutions found to be of any practical relevance they have to be easily obtained from a reasonable range of input light conditions being little sensitive to deviations in the fields transverse profile or amplitudes or relative phases. The numerical results in [87]-[89] show that this is actually the case for the solitons existing in nonlinear quadratic structures. The present study is restricted therefore to provide a general overview of the features of the dynamics of soliton excitation that provide direct insight into the phenomena discussed hereafter.

In nonintegrable nonlinear systems such as the one analyzed here, the problem of trying to predict which electromagnetic energy distribution will a given fields input evolve into, becomes a question if not impossible, very difficult to answer.

When trying to decide whether a given input fields distribution will evolve into a soliton or else spread as a linear wave, the tool which readily comes to the analysis is the *effective beam width* defined as

$$\theta = \int_{-\infty}^{\infty} s^2 \left[\frac{2}{r} |a_1|^2 + \frac{1}{\alpha} |a_2|^2 \right] ds. \tag{3.95}$$

Evaluation of its second derivative with respect to the propagation variable is expected to give

a clue on which the evolution may be, provided that by using the governing equations one is capable of expressing it in terms of the conserved quantities in the system for obtaining a kind of *Virial Theorem* applicable to the $\chi^{(2)}$ case. For given input fields that make $d^2\theta/ds^2$ positive, the expected tendency is spreading while if it is negative then there is a chance for keeping it constant and hence forming a soliton. One readily obtains

$$\frac{d^2\theta}{d\xi^2} = -8\mathcal{H} - 4\frac{\mathcal{J}}{I} - 3\int_{-\infty}^{\infty}\left((a_1^*)^2 a_2 + a_1^2 a_2^*\right) ds + \frac{2}{\alpha}\delta\int_{-\infty}^{\infty} s\left((a_1^*)^2 a_2 + a_1^2 a_2^*\right) ds + \frac{2}{\alpha}\delta^2 I_2. \quad (3.96)$$

Not even in the absence of walk-off a complete expression in terms of conserved quantities is found whereupon evaluation of $d^2\theta/ds^2$ for the input fields is not expected to provide any valuable information as for soliton formation or spreading. Besides that, there is the amazing capability of the beams inside the crystal for quick reshaping with little radiation emission that may all of a sudden transform a fields distribution with nothing in common with a stationary solution in something very close to it. See for example Figure 3-12.

Hence, one can only aspire to get some intuition on which are the options generically chosen by the dynamics for to some extent get a clue on which are the most likely possibilities. Hereof, the leading role of numerical simulation in the dynamic evolution analysis issue. Given the complexity of the problem, initially the study is restricted to configurations with negligible walk-off and bright symmetric input conditions so that all beams are likely to follow the straight direction if not splitted up symmetrically forming several solitons.

A numerical beam propagation algorithm based upon a modified symmetrized split-step Fourier method whose principles are briefly outlined in section 2.4, provides the outputs upon which the analysis relies.

One of the colored lines showing the fields evolution over the $I - \mathcal{H}$ plane in Figure 3-12 corresponds to *Sech* like profiles while the other is for $Sech^2$ profiles. The significant difference in terms of transverse profile dependencet does not result quite reflexed in the evolution undergone over the $I - \mathcal{H}$ plane provided the fields start from very close points. Having that into account and unless stated otherwise, all simulations will generally correspond to *Sech* like profiles.

Aimed at demonstrating the stability of the solutions, monitorization of the dynamics has already been successfully accomplished through motion in the $I - \mathcal{H}$ plane. However useful

because the features of stability are also reflected in the plane, it does not quite evidence the oscillating behavior displayed by the solitary wave solutions.

Seeking for other approaches to investigate the dynamics, *Stokes parameters* have often been successfully resorted to to provide useful pictures of evolution. In the $\chi^{(2)}$ case defined as

$$\begin{aligned} S_0 &= \int_{-\infty}^{\infty} \left[|a_1|^2 + |a_2|^2 \right] ds, \\ S_1 &= \int_{-\infty}^{\infty} \left[|a_1|^2 - |a_2|^2 \right] ds, \\ S_2 &= \int_{-\infty}^{\infty} \left[\frac{a_1^2 a_2^* + \left(a_2^*\right)^2 a_2}{|a_1|} \right] ds, \\ S_3 &= -\int_{-\infty}^{\infty} \left[\frac{a_1^2 a_2^* - \left(a_2^*\right)^2 a_2}{|a_1|} \right] ds, \end{aligned} \tag{3.97}$$

are susceptible of providing any direct and valuable information only if the fields verify

$$a_\nu(s,\xi) = \Theta_\nu(\xi)\,\Sigma_\nu(s), \tag{3.98}$$

and $\Sigma_1 = \Sigma_2$ which only happens for configurations in which the wavevector mismatch is close to zero. Under these assumptions the $\{S_\nu\}$ set may be written

$$\begin{aligned} S_0 &= \left(|\Theta_1|^2 + |\Theta_2|^2 \right) \int \Sigma^2((s))\, ds, \\ S_1 &= \left(|\Theta_1|^2 - |\Theta_2|^2 \right) \int \Sigma^2((s))\, ds, \\ S_2 &= \frac{\Theta_1^2 \Theta_2^* + \left(\Theta_1^*\right)^2 \Theta_2}{|\Theta_1|} \int \Sigma^2((s))\, ds, \\ S_3 &= -j \frac{\Theta_1^2 \Theta_2^* - \left(\Theta_1^*\right)^2 \Theta_2}{|\Theta_1|} \int \Sigma^2((s))\, ds, \end{aligned} \tag{3.99}$$

verifying

$$S_1^2 + S_2^2 + S_3^2 = S_0, \tag{3.100}$$

so that it defines a Poincaré Sphere but only under the specific conditions stated above.

The restrictions encountered advice search of more efficient expressions of the parameters which while still providing a useful picture of the dynamics are applicable to a broader range of situations. Attending to the results, resorting to *differential Stokes parameters*, namely the set $\{s_\nu\}$ defined through

$$S_\nu(\xi) = \int s_\nu(\xi, s)\, ds, \tag{3.101}$$

appears as the most natural way to proceed. To eliminate the transverse coordinate dependence these parameters are evaluated at the beams peak, $s = 0$, so that writing the fields in the form

$$a_\nu(s,\xi) = U_\nu(s,\xi)\exp\left(j\psi_\nu(s,\xi)\right),$$

with U_ν, ψ_ν real functions, it is obtained in the most general case

$$s_0 = U_1^2 + U_2^2, \tag{3.102}$$

$$s_1 = U_1^2 - U_2^2, \tag{3.103}$$

$$s_2 = 2U_1U_2\cos\left(2\psi_1 - \psi_2\right), \tag{3.104}$$

$$s_3 = 2U_1U_2\sin\left(2\psi_1 - \psi_2\right). \tag{3.105}$$

These redefined set of parameters is readily shown to verify

$$s_1^2 + s_2^2 + s_3^2 = s_0^2, \tag{3.106}$$

a Poincaré sphere of radius s_0 which somehow represents the local energy contained in the beams peak, in the three parameters space defined by $\{s_1, s_2, s_3\}$. A normalization is often used so that

$$\tilde{s}_1^2 + \tilde{s}_2^2 + \tilde{s}_3^2 = 1, \tag{3.107}$$

and the sphere has unity radius.

Based on the above, evolution from different input conditions over the Poincaré sphere will be used to illustrate typical behaviors encountered in the dynamics. It is useful therefore to identify in the $\{s_1, s_2, s_3\}$ three dimensional space the locus of the families of bright stationary solutions found in the absence of walk-off for which one has

$$\psi_2 = 2\psi_1, \tag{3.108}$$

and hence

$$s_0 = U_1^2 + U_2^2, \tag{3.109}$$

$$s_1 = U_1^2 - U_2^2, \tag{3.110}$$

$$s_2 = 2U_1U_2, \tag{3.111}$$

$$s_3 = 0. \tag{3.112}$$

To this aim it is helpful to use the first integral of the governing equations. With $A_\nu(\xi) = U_\nu(0,\xi)$ it may be expressed

$$A_1^2 = \frac{(2\kappa_1 + \beta) A_2^2}{2(A_2 - \kappa_1)}. \tag{3.113}$$

For $\beta = 0$, and using the self-similarity transformations (3.22) one gets

$$\frac{A_1^2}{A_2^2} = \frac{2}{2(A_2(\kappa_1 = 1) - 1)}. \tag{3.114}$$

From the numerical shooting method it is obtained

$$A_2(\beta = 0, \kappa_1 = 1) \simeq 1.68652, \tag{3.115}$$

leading to

$$\widetilde{s}_1(\beta = 0) \simeq 0.18587, \tag{3.116}$$

$$\widetilde{s}_2(\beta = 0) \simeq 0.98257, \tag{3.117}$$

whereupon by means of this single point in the $\{\widetilde{s}_1, \widetilde{s}_2, \widetilde{s}_3\}$ space the stationary solutions for $\beta = 0$ and any energy flow are represented.

In the $\beta \neq 0$ case one has the expressions

$$\widetilde{s}_1 = \frac{4\kappa_1 + \beta - 2A_2}{2A_2 + \beta}, \tag{3.118}$$

$$\widetilde{s}_2 = \frac{2\sqrt{2\kappa_1 + \beta}\sqrt{2(A_2 - \kappa_1)}}{2A_2 + \beta}. \tag{3.119}$$

Different points in the Poincaré sphere will clearly be obtained for any total power as corresponding κ_1 different values are considered. For very high κ_1, since β may be neglected from the stationary equations, the loci of the families of bright stationary solutions for $\beta \neq 0$ must

converge to the $\beta = 0$ family point, as Figure 3-13 shows.

The lower cutoff values are easily found by noticing

$$\widetilde{s}_1 (\beta > 0)|_{\text{cut off}} = \lim_{\substack{\kappa_1 \to 0 \\ A_2 \to 0}} \frac{4\kappa_1 + \beta - 2A_2}{2A_2 + \beta} = 1, \tag{3.120}$$

$$\widetilde{s}_1 (\beta < 0)|_{\text{cut off}} = \lim_{\kappa_1 \to -\beta/2} \frac{4\kappa_1 + \beta - 2A_2}{2A_2 + \beta} = -1. \tag{3.121}$$

The cut off values then yield

$$\beta > 0 \longrightarrow \widetilde{s}_1 = 1,\ \widetilde{s}_2 = 0, \tag{3.122}$$

$$\beta < 0 \longrightarrow \widetilde{s}_1 = -1,\ \widetilde{s}_2 = 0. \tag{3.123}$$

Another interesting point in the sphere is given by the analytical solution occurring for $\beta = -3$. One has

$$\widetilde{s}_1 = -1/3, \tag{3.124}$$

$$\widetilde{s}_2 = \frac{2\sqrt{2}}{3}. \tag{3.125}$$

All points and locus identified are schematically shown in Figure 3-13.

In practice, since the beams evolution involves continuous changes in the peaks local energy which are interesting in the investigation and however go unnoticed in the normalized form of the parameters, it is chosen to monitor the evolution in the unnormalized $\{s_1, s_2, s_3\}$ space. As seen in Figure 3-14, the three dimensional space picture provided by the unnormalized set of parameters allows for simple characterization of the different excitation conditions that can be considered and the possible chances to reach a stationary state in terms of proximity to the corresponding bright family stationary solution branch. The superimposed sphere represents the amount of total power injected in such a way that the stationary states eventually reached are necessarily held into it.

The unnormalized cutoff values are

$$s_1 (\beta > 0)|_{\text{cut off}} = \lim_{\substack{\kappa_1 \to 0 \\ A_2 \to 0}} \left(A_1^2 - A_2^2\right) = 0, \tag{3.126}$$

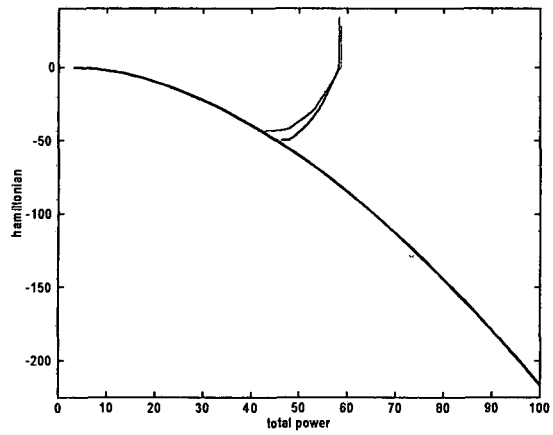

Figure 3-12: Examples of evolution over the I-$\mathcal{H}$ plane for $\beta = -3$ and for $Sech$ ('m') and $Sech^2$ ('g') profiles. Color scale as in App. B.

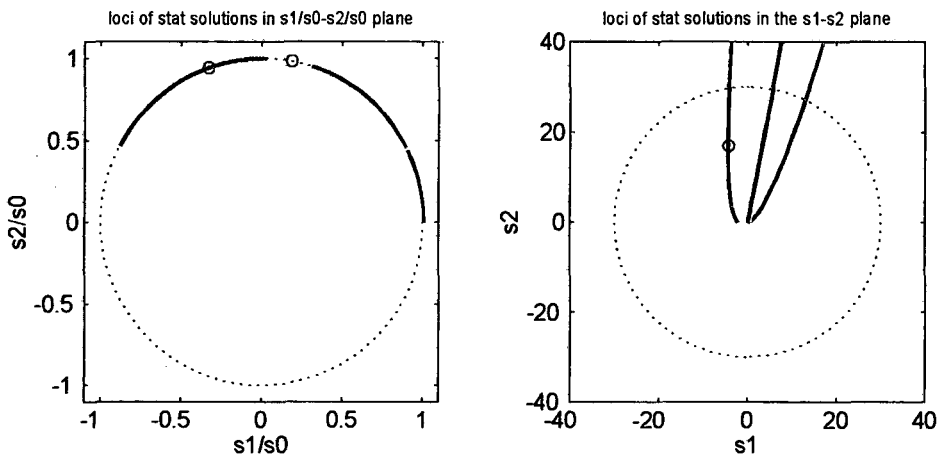

Figure 3-13: Loci of the stationary bright solutions for $\delta = 0$ in the $s_1 - s_2$ normalized (left) and unnormalized (right) plane. ('bk'): $\beta = 0$, ('g'): $\beta = -3$, ('m'): $\beta = 3$. The point in blue indicates the position of the analytic solution. Color scale as in App. B.

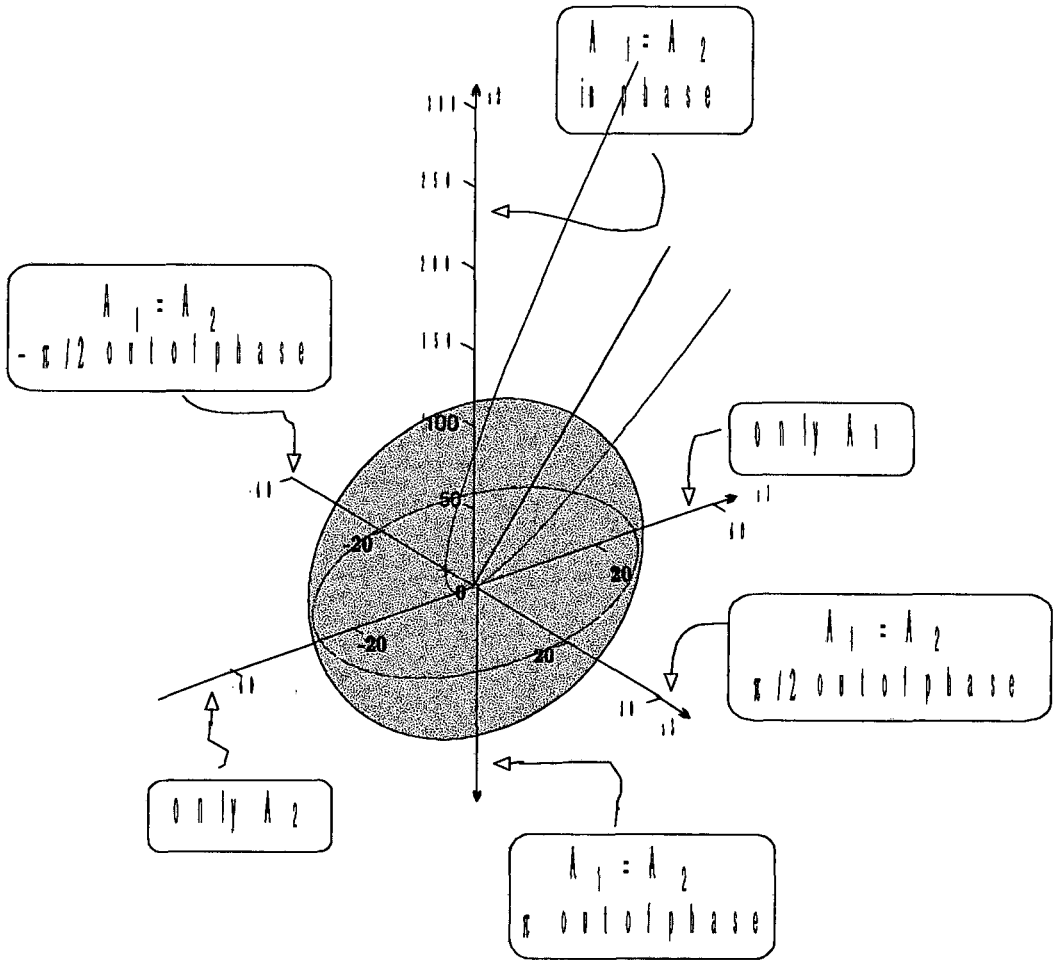

Figure 3-14: Three dimensional Stokes parameters space showing location of different excitation conditions, the loci of stationary solutions for ('bk'): $\beta = 0$, ('g'): $\beta = -3$, ('m'): $\beta = 3$ and the Poincaré sphere. Color scale as in App. B.

$$s_2\left(\beta>0\right)|_{\text{cut off}}=\lim_{\substack{\kappa_1\to 0\\ A_2\to 0}} 2A_1A_2=0, \tag{3.127}$$

$$s_1\left(\beta<0\right)|_{\text{cut off}}=\lim_{\kappa_1\to -\beta/2}\left(A_1^2-A_2^2\right)=\lim_{\kappa_1\to -\beta/2}\left(\frac{(2\kappa_1+\beta)}{2\left(A_2-\kappa_1\right)}A_2^2-A_2^2\right). \tag{3.128}$$

To solve for this limit take into account the second derivative values at the $s=0$ point which for bright stationary profiles need to be negative. From the stationary equations get

$$U_{1_{ss}}|_{s=0}=\frac{2}{r}A_1\left(A_2-\kappa_1\right), \tag{3.129}$$

$$U_{2_{ss}}|_{s=0}=\frac{2}{\alpha}\left(A_1^2-\kappa_2A_2\right). \tag{3.130}$$

Using the first integral (3.113)

$$U_{1_{ss}}|_{s=0}=\frac{2}{r}A_1\frac{\kappa_2}{2}\frac{A_2^2}{A_1^2}=\frac{\kappa_2}{r}\frac{A_2^2}{A_1}, \tag{3.131}$$

$$U_{2_{ss}}|_{s=0}=\frac{2}{\alpha}\left(\frac{\kappa_2}{2}\frac{A_2^2}{\left(A_2-\kappa_1\right)}-\kappa_2A_2\right)=\frac{\kappa_2A_2}{\alpha\left(A_2-\kappa_1\right)}\left(2\kappa_1-A_2\right). \tag{3.132}$$

Nonzero second derivatives when $\kappa_1\to -\beta/2$, $\kappa_2\to 0$, require vanishing denominators in the above expressions, hence

$$A_1\underset{\kappa_2\to 0}{\longrightarrow}0, \tag{3.133}$$

$$A_2\underset{\kappa_2\to 0}{\longrightarrow}\kappa_1\,. \tag{3.134}$$

That helps to resolve the limit in (3.128) and obtain the unnormalized cutoff value for $\beta<0$ that follows

$$\lim_{\kappa_1\to -\beta/2}\left(\frac{2\kappa_1+\beta}{2\left(A_2-\kappa_1\right)}A_2^2-A_2^2\right)=\lim_{\kappa_1\to -\beta/2}\left(\frac{4\kappa_1+\beta-2A_2}{2\left(A_2-\kappa_1\right)}A_2^2\right)=\lim_{\kappa_1\to -\beta/2}\left(-2A_2^2\right)=-\frac{\beta^2}{4}. \tag{3.135}$$

In Figures 3-15-3-19 some representative examples of evolution in the three dimensional unnormalized Stokes space are shown.

All cases where a soliton is finally formed feature a quite fast phase locking condition achievement reflected in the fact that very quickly they reach the $s_2\simeq 0$ area in the three

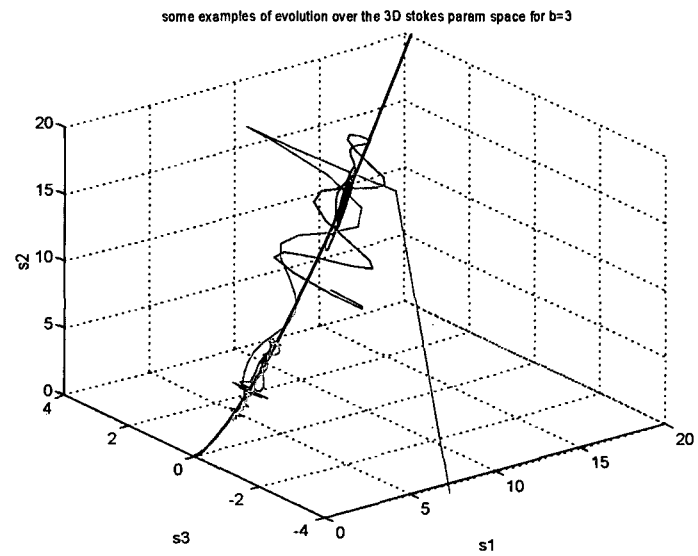

Figure 3-15: Examples of evolution up to 500 normalized propagation distances over the three dimensional Stokes Parameters space for $\beta = 3$. ('c'): splitting case for $A_1 = 4$, $A_2 = 1$ and π relative phase; ('m' and 'b'): respectively $I = 10$ and $I = 25$ with amplitudes that realize a minimum of hamiltonian. The curve in black shows the loci of stationary solutions for this wavevector mismatch value.

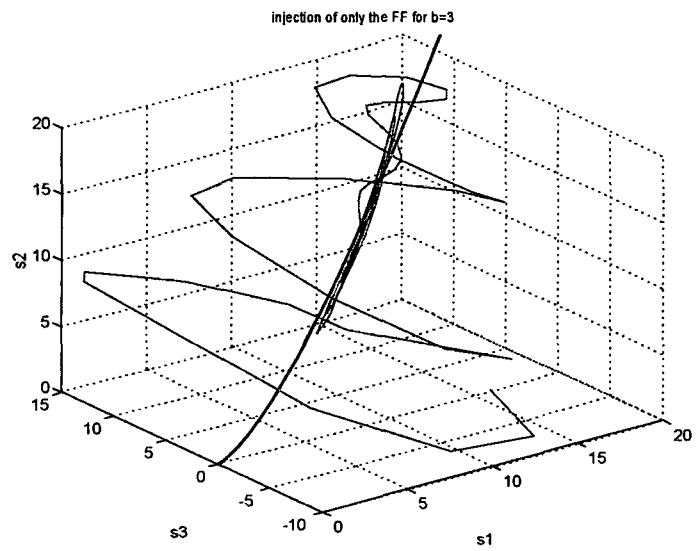

Figure 3-16: Same as previous figure considering injection of the fundamental field only $A_1 = 4$.

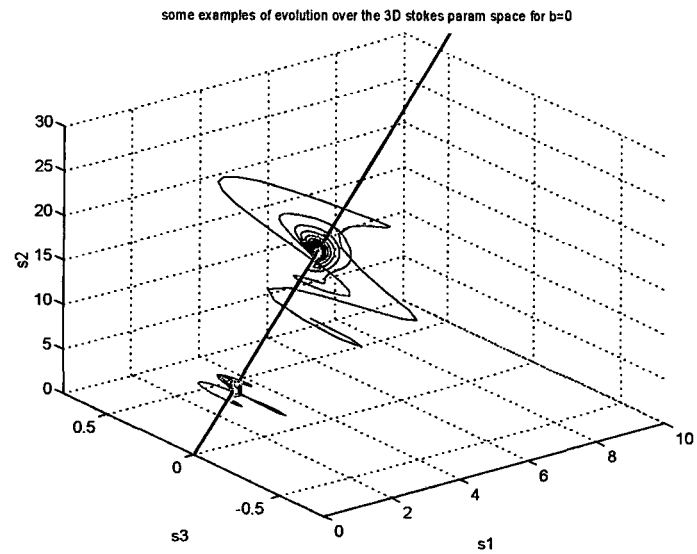

Figure 3-17: Examples of evolution up to 500 normalized propagation distances over the three dimensional Stokes Parameters space for $\beta = 0$. ('m' and 'b'): respectively $I = 10$ and $I = 25$ with amplitudes that realize a minimum of hamiltonian.Color scale as in App. B.

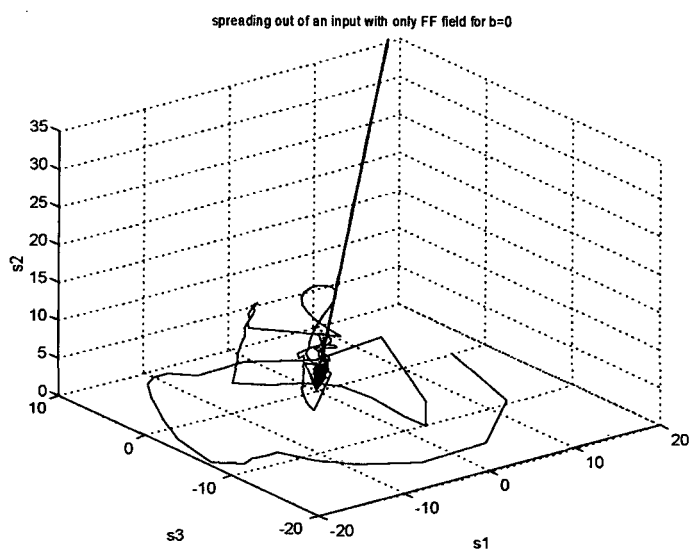

Figure 3-18: Same as previous figure illustrating the spreading out of the beam when only the fundamental field has been injected, $A_1 = 4$.

dimensional Stokes space and then they start swirling around the stationary solitary waves curves reducing in every turn the radius of the swirl.

The robustness of the soliton formation process is evidenced by the fact that the stationary solutions curve is reached from very distant points in the three dimensional Stokes space. Special attention deserves the evolution in cyan line in Figure 3-15 corresponding to a case where the input beam results splitted up into two solitons travelling in opposite directions with respect to the z axis as a result of the input π phase difference between the harmonics. Exact representation of the fields propagation and explanation of such a behavior is found in section 6.2, see Figure 6-32, but the interesting remark here is the steady evolution of the Stokes parameters evaluated at the peak over the long path that separates the input conditions from the stationary solutions curve.

Also it is worth emphasizing the fact that when only the fundamental is input, for the same input conditions featuring a reasonably high amount of input power, the system is able to reach a solitary wave state if $\beta = 3$, but the beams completely spread out for $\beta = 0$ and even a more terrible spreading out result is obtained when $\beta < 0$. This can of course be connected with the fact that as β is made larger a lower second harmonic content is required in the stationary solution which certainly eases the reaching of a stationary state, but the case when only the fundamental is input reveals itself as a rather interesting one with special characteristics as for the formation of solitons which deserve to be analyzed in more detail as it is next done.

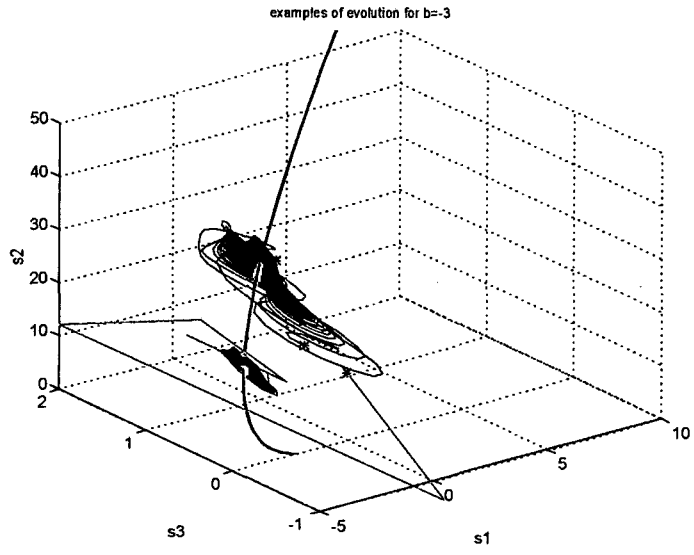

Figure 3-19: Examples of evolution over the Stokes parameters space for $\beta = -3$. In both cases the amplitudes have been chosen so to yield a minimum of hamiltonian ('g'): $I = 25$ and 1200 normalized propagation distances; ('m'): $I = 40$ and 500 normalized propagation distances. Stars in red and blue indicate respectively the starting and finishing points.

3.6.2 SH generation with no SH input

Suggested by the large wavevector mismatch NLSE limit and confirmed through numerical simulations is the accepted fact that for positive β inputs at the fundamental frequency are in a wide range of situations capable of generating the required second harmonic and form a solitary wave. This section is devoted to analyze how these process takes place through deep insight into the dynamics.

Right after the fundamental field has been launched into the waveguide, in the very first step of the beam propagation algorithm a second harmonic signal appears whose phase invariably regardless of fundamental power launched, wavevector mismatch or even walk-off parameter approaches the $\pi/2$ value.

This phenomenon is explained through the amplitude-phase description presented in section 2.3.5, (2.113), (2.114), (2.119), (2.120). The fact that no second harmonic signal is present at the waveguide input, i.e. the $\xi = 0$ point, entails that some functions as ψ_2 and $\Delta\psi$ become meaningless at that point. Nevertheless, as soon as the fields enter the waveguide, say at the $\xi = 0^+$ point, a differential quantity of second harmonic is generated out from the fundamental. As no sudden changes in phase are expected to occur in the differential distance considered and since $\psi_1(\xi = 0^+) \approx \psi_1(\xi = 0) = 0$, this is indicative of the fact that $\psi_2(\xi = 0^+) \neq 0$ yielding $\Delta\psi(\xi = 0^+) < 0$ and significant energy transfer from fundamental to second harmonic.

In absence of second harmonic input, from (2.120) one obtains

$$\psi_{2_\xi}(\xi = 0^+) \simeq \frac{U_1^2(\xi = 0^+)}{U_2(\xi = 0^+)} \cos\left(\Delta\psi(\xi = 0^+)\right) = \frac{U_1^2(\xi = 0^+)}{U_2(\xi = 0^+)} \cos\left(\psi_2(\xi = 0^+)\right). \quad (3.136)$$

Writing the second harmonic transverse profile as

$$U_2(\xi = 0^+) \simeq U_2(\xi = 0) + U_{2_\xi}(\xi = 0^+)\, d\xi, \quad (3.137)$$

with $d\xi$ the differential distance between $\xi = 0^+$ and $\xi = 0$, since $U_2(\xi = 0) = 0$, one gets

$$U_2(\xi = 0^+) \simeq -U_1^2(\xi = 0^+) \sin\left(\Delta\psi(\xi = 0^+)\right) d\xi = U_1^2(\xi = 0^+) \sin\left(\psi_2(\xi = 0^+)\right) d\xi, \quad (3.138)$$

Combination of (3.138) with (3.136) yields

$$\psi_{2_\xi}\left(\xi = 0^+\right) d\xi = \frac{\cos\left(\psi_2\left(\xi = 0^+\right)\right)}{\sin\left(\psi_2\left(\xi = 0^+\right)\right)}. \tag{3.139}$$

Assuming $\psi_{2_\xi}\left(\xi = 0^+\right)$ is finite it is concluded that

$$\frac{\cos\left(\psi_2\left(\xi = 0^+\right)\right)}{\sin\left(\psi_2\left(\xi = 0^+\right)\right)} \approx 0, \tag{3.140}$$

whereupon either it is $\psi_2\left(\xi = 0^+\right) \approx \pi/2$ or else $\psi_2\left(\xi = 0\right) \approx \psi_2\left(\xi = 0^+\right) \approx -\pi/2$, both corresponding to the same result for a_2 since the apparent π difference is compensated through the change of sign caused upon the amplitude to yield in both cases $a_2 = U_2 \exp\left(j\pi/2\right)$.

The second harmonic phase calculated through the beam propagation method confirms the validity of the above derivation showing immediate reaching of a value very close to $\psi_2 = \pi/2$.

Fast evolution towards the stationary state is favoured for large positive phase mismatches not only because the stationary solution features a greater fundamental energy content but also because quick detachment from the initial $\Delta\psi \simeq -\pi/2$ towards reaching of the phase locking condition, $\Delta\psi \simeq 0$ is allowed. Conversely for negative β values, not only the stationary solution second harmonic content is higher but also it has to be reached starting from initial $\Delta\psi \simeq -\pi/2$ being pulled away from $\Delta\psi \simeq 0$ towards more negative values.

3.6.3 Intuitive view of the evolution

So far, it has become evident how hard it results the proposed task of identificating the input conditions that are likely to end up forming a soliton and those which will more probably lead to beams spreading out. The amazing capability of quick reshaping featured by the beams propagating inside the nonlinear crystal makes necessary a whole detailed study of each specific case to be carried out in order to try to recognize which are the main drivers of propagation responsible for formation or spreading out, efficient coupling of energy or high amounts of radiation.

Nevertheless, as the features of the long term propagation are to a great extent determined by the dynamics of evolution in the very first stages, some intuitive insight can be gained by analyzing the main effects expected to be of relevance in these first stages. Through detailed

study of many different cases one is able to develop a certain expertise on which are the options usually chosen by the dynamics and may try to derive a simple intuitive model that helps to understand, and in some cases to foresee the main characteristics the behaviour followed by the beams inside the crystal and the outputs that are likely to be obtained. In the present section an intuitive analysis of the features of the fields propagation from different input conditions is carried out which tries to elucidate the main mechanisms taking part in the dynamics. Given the enormous complexity of the system it is only pretended to derive a few guidelines that may help to give an approximate idea of the nature and basic characteristics of the evolution while under certain conditions be useful to predict to some extent the main features of the final state reached.

As suggested by the numerics and already outlined in the previous qualitative description of stationary solutions, in the process of evolution towards an stationary state two simultaneous major effects can be distinguished, namely interharmonics energy exchange aimed at achieving into each individual transverse point a peak amplitude relation which through nonlinear phase matching maintains interharmonics energy exchange within certain limits on one side, and on the other, energy dragging which is in charge of redistributing the energy throughout the profile so that by altering the local energy value into the particular transverse points it alters the energy exchange rate in such a way that the combined effect of both interharmonics energy exchange and energy dragging progressively flattens the phase profiles down.

Since through the cases of fields evolution studied so far, fast reaching of approximate nonlinear phase matching in the beams peak seems to be decisive as for successful soliton formation, the analysis considers in the first place the dynamics of achievement of a proper peak amplitude relation through interharmonics energy exchange.

Nonlinear phase matching by interharmonics energy exchange

As for characterization of nonlinear phase matching progressive reaching in the profiles peak in the first steps of propagation, two are the key factors to take into account, namely the value of β with direct influence upon the $\Delta\psi$ value, recall (3.88)

$$\Delta\psi_\xi = \frac{U_{1ss}}{U_1} - \frac{1}{4}\frac{U_{2ss}}{U_2} + 2U_2\cos(\Delta\psi) - \frac{U_1^2}{U_2}\cos(\Delta\psi) + \beta = 0, \tag{3.141}$$

and the peak's local energy content or more exactly the peak's amplitudes product $U_1^2 U_2$ determining the energy exchange rate and therefore the system's capability of peaks amplitude variation to compensate through the nonlinear or amplitude terms in (3.141), third and fourth, the constant monotonic tendency imposed by β on the nonlinear phase mismatch.

The plots in Figure 3-20 give illustration of the role played by the total energy flow which basically as getting bigger accelerates the energy exchange between harmonics so that the amplitude relation realizing the nonlinear phase matching is achieved in few energy exchange periods. From here it steams that for initial A_1/A_2 peak relations very far away from the stationary value enough energy needs to be supplied so to allow for quick enough amplitude compensation before the solution evolves too much away from equilibrium, see the example in Figure 3-21.

That is understood in terms of the Stokes three dimensional space as a larger radius of the Poincaré sphere required for a too long and tortuous evolution trajectory, or in the $I - \mathcal{H}$ plane picture as larger I values needed for the initial conditions point to fall to the right side of the stationary solutions curve in the plane.

In Figure 3-21, since for the positive β value considered lower energy flow values correspond to higher A_1/A_2 peak relation, to compensate for the difference and establish a more fair comparison, for the lower energy value, a higher initial amplitude relation has been used.

As for wavevector mismatch dependence of the evolution towards nonlinear phase matching it may be said that as evidenced by the examples in Figure 3-22, high $|\beta|$ values determine initially a $\Delta\psi$ fast monotonic tendency yielding very short energy exchange periods. Thus for high energy values a lot of energy is transferred between harmonics leading from phase mismatch of one sign swiftly to phase mismatch of the opposite sign whereupon a lot of energy exchange periods are required to achieve the proper amplitude relation that ensures nonlinear phase mismatch.

For a correct interpretation of the plots in Figures 3-20, 3-22 recall that the energy exchange rate depends on the product $U_1^2 U_2$ and for example in Fig. 3-22 as β increases, as increasing the stationary A_1/A_2 peak relation, considering a minimum of the hamiltonian for the initial amplitude values entails a higher energy exchange rate, hence the decrease in the amplitude of the oscillations observed.

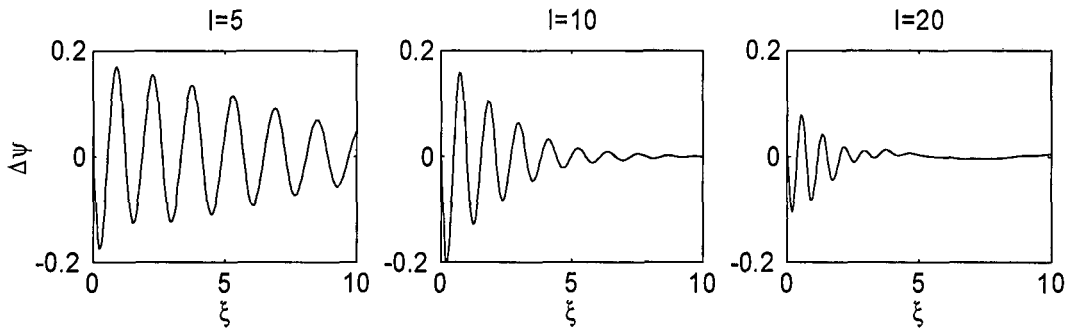

Figure 3-20: Nonlinear phase matching achievement for different initial energy flow values. In all cases $\beta = 3$ and the amplitudes have been chosen to realize a minimum of the hamiltonian.

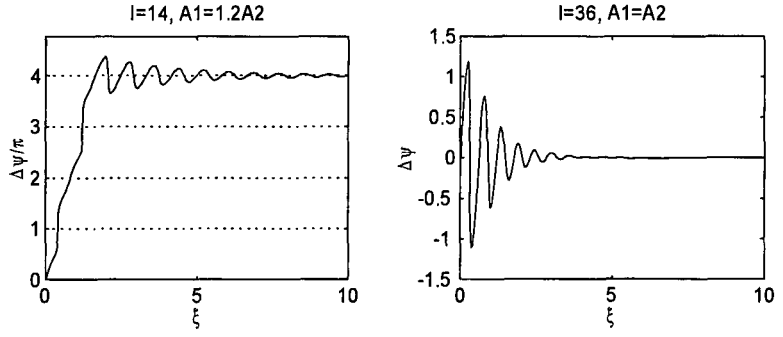

Figure 3-21: Examples of nonlinear phase mismatch evolution for $\beta = 6$ and different initial energy flow values.

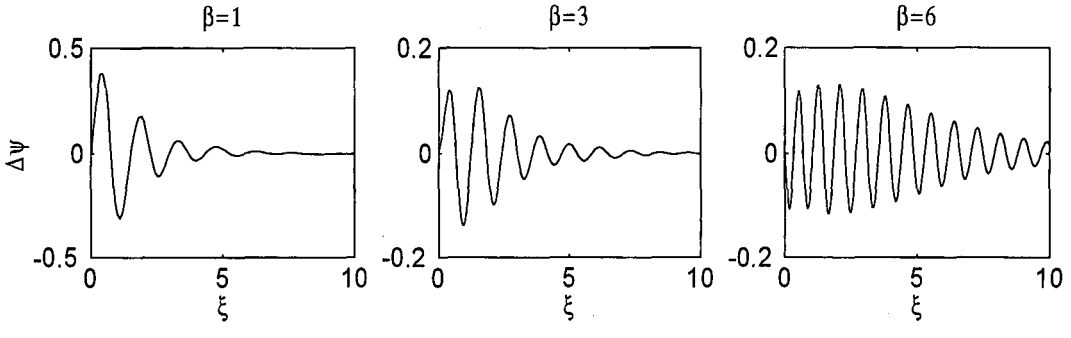

Figure 3-22: Nonlinear phase matching achievement for different values of the wavevector mismatch, $I = 10$ and amplitude values that feature a minimum of hamiltonian.

Redistribution of energy by energy dragging

In the course of evolution, the energy belonging to each harmonic is continuously being redistributed along the transverse variable following the transverse phase gradients in what was identified and referred to as internal transverse energy flux in such a way that when a solitary wave is formed an equilibrium is reached so to maintain constant phase fronts verifying, recall (3.89-3.90),

$$\kappa_1 = \frac{1}{2}\frac{U_{1_{ss}}}{U_1} + U_2, \tag{3.142}$$

$$\kappa_2 = \frac{1}{4}\frac{U_{2_{ss}}}{U_2} + \frac{U_1^2}{U_2}, \tag{3.143}$$

where the solitary wave is taken to travel in the straight direction. The first terms in the right hand side, diffraction terms, must be such that they quickly enough compensate amplitude variations due to eventual energy dragging before alterations in the interharmonics energy exchange velocities further worsen the situation causing more energy dragging of the same direction.

For usual energy levels, energy dragging in the first steps of propagation is mainly governed by the amplitudes terms in (3.142-3.143) and therefore it is very sensitive to the differential energy exchange velocities occurring in different parts of the profile having different local energies. Since more energetic parts of the profile exchange energy faster this effect basically causes through further sharpening of the peaks in the growing harmonic an enhanced focusing in the decreasing one due to increase in its phase nonlinear term and viceversa, by smoothing down the profile in the decreasing harmonic it induces some tendency to defocus in the growing harmonic provided enough amplitudes compensation through interharmonics energy exchange has taken place so that $\Delta\psi$ can be kept within the range $-\pi/2 < \Delta\psi < \pi/2$, i.e. $\cos(\Delta\psi) > 0$, and the nonlinear parametric contributions to the phases are positive. Excesses of local energy into specific transverse points translate into too fast energy exchange between harmonics when compared with that having place in the neighboring transverse points in such a way that the growing harmonic since its phase profile basically depends through the parametric interaction upon the decreasing harmonic amplitude value tends to drag local energy out of the transverse point under consideration and viceversa for the decreasing harmonic. Considering that the

amount of energy dragged into or out the specific transverse point is roughly proportional to the square of the amplitude value of the corresponding harmonic, see (2.119-2.120), it follows that the harmonic who is too quickly growing will drag more energy out than the decreasing harmonic is capable of dragging into the transverse point. Thus the local energy excess is relieved by causing some loss in too fast exchanging energy transverse points which is delivered to its too slow energy exchanging neighbors by which process the equilibrium between interharmonics energy exchange and energy dragging is restored.

It may then be said that the energy dragging process plays here a kind of 'Robin Hood' role by taking away from the rich and delivering to the poor in terms of redistribution of energy, for the sake of homogeneity of local energy exchange rates throughout the transverse profile. Figure 3-23 obtained by standard split-step Fourier beam propagation method for equations (2.94) is an example of how differential energy dragging in both harmonics redistributes the energy along the transverse coordinate so that all transverse profile points rhythms of energy exchange both between harmonics and with other transverse points are properly matched so that finally the two harmonics agree to exchange energy rhythmically forming an *oscillating state*, see Figure 3-23.

3.6.4 Oscillating states

Basically trough the parametric interaction terms, the combined effect of interharmonics energy exchange and alternating energy dragging inside each harmonic, lead every transverse point close enough to the nonlinear phase matching, i.e. $\Delta\psi = 0$, and with such a content in local energy that the two harmonics behave almost as a unit undergoing simultaneously focusing and defocusing intervals on propagation accompanied by respective interharmonics energy exchange periods whose sign depends on that of the phase mismatch value, in a periodic manner so that each time the fields distribution falls closer to a stationary solution. One may then say that they are *locked* to each other forming an *oscillating state*. For example for $\beta < 0$, since with an increase in local energy a higher U_1/U_2 relation is needed, to a focusing period corresponds an energy exchange period from second harmonic to fundamental as it has been confirmed by launching the analytic solution and propagating it with a numerical split step Fourier bpm for equations (2.94), see Figure 3-25. Analogously for $\beta > 0$ the focusing periods coincide with

energy exchange from fundamental to second harmonic as an increase of local energy in center requires a lower U_1/U_2 relation.

These oscillating states arise as a consequence of the difference between the interharmonics energy exchange and energy dragging rates or equivalently, between nonlinear interaction and diffraction typical variation lengths, and the mismatch between initial and stationary amplitude values, and initial and stationary transverse profiles.

Consider for example the frequent situation in which as a consequence of local energy differences, after the first steps of propagation more energetic center has achieved nonlinear phase matching while the wings though close, still have $\Delta\psi \neq 0$. Lower contribution of nonlinear parametric interaction terms in tails to the phase front value due to multiplication by $\cos(\Delta\psi)$ factor, see expressions (2.119-2.120), causes the energy there to be dragged towards the center which in order to assimilate the increase of energy will be forced to temporarily abandon the nonlinear phase matching for an amplitudes relation rearrangement. Since the center is receiving twice the energy the tails are losing, eventually the $\Delta\psi$ deviation from equilibrium leads to a more reduced effect of nonlinear parametric interaction in center than in tails which added to the action of linear diffraction terms whose contribution to the phase constants is becoming more negative in the peak that sharpens and more positive in tails which result smoothed down, causes the energy dragging process to reverse its direction so that energy starts to be dragged from center to tails during the amplitudes rearrangement and recovering of equilibrium period undergone by the profiles peak.

For bright initial profiles and initial amplitudes reasonably close to the stationary values, since interharmonics energy exchange process is faster than energy dragging and therefore the equilibrium in center is restored before all energy dragged into the center during the period of focusing is recovered by the tails through the energy dragging mechanism, the new equilibrium point for center is likely to occur in a higher local energy value than in beginning of focusing period. Hence faster $\Delta\psi = 0$ condition recovering in next defocusing period will reduce the amount of local energy being dragged out from the profiles peak. Through this sequence the transversal energy fluxe progressively gets reduced giving rise to the damped breathing of peak values observed for the solitary wave solutions excited with bright profiles. Figure 3-24.

The key condition for the oscillations to get damped is that interharmonics energy exchange

really is faster in recovering the $\Delta\psi = 0$ equilibrium than energy dragging in stealing the center energy. That happens when the U_1/U_2 relation in center corresponds to a local energy value slightly higher than that belonging to the actual total power contained in the solution or in other words, when the locking is achieved with a sharper profile than that of the stationary solution corresponding to the peak values. Thus it is ensured that in the profiles peak the strength of the energy exchange process together with the negative contribution of linear diffraction terms as the sharpening takes place, relieves on time the excesses of local energy produced during the focusing periods thus preventing fatal phase locking destabilizations. The period and amplitude of the oscillations depends basically on the rate of local energy exchange as compared to that for energy dragging, being both determined by the initial conditions and the wavevector mismatch.

Hence, when starting with bright amplitude profiles since more energetic center thanks to faster energy exchange manages to achieve sooner the correct amplitude values for proper and exact locking to $\Delta\psi = 0$ condition and therefore start focusing significantly in initial steps of the propagation, formation of an oscillating state as the ones discussed above and illustrated in Figure 3-24 appears as the more natural evolution, which thus confirms the robustness of the soliton formation process and its usefulness in practical setups.

On the contrary, starting with amplitude values in complete disagreement with the stationary ones, initially diffraction prevails over nonlinear parametric interaction whereupon more energetic center tends to lock to U_1/U_2 relations which correspond to lower local energy in center than the required for the total power contained in the system or in other words, the locking is realized with a too broad transverse profile. Once locked, since the tails still are too much away from $\Delta\psi = 0$ condition, energy is focused towards center causing such a great avalanche of energy that the $\Delta\psi$ deviation thus brought about will be too much slowly recovered by too low energetic (when compared to the total energy in the system) center. Thus, the effect of energy dragging outweighs that of nonlinear parametric interaction in such a way that the center after each energy dragging period locks to U_1/U_2 relations corresponding to lower local energy values till eventually the tails thanks to the progressive injection of power are able to get close enough to $\Delta\psi = 0$ condition so that finally all energy is swept away from center and complete beam break-up takes place as it has been verified through the numerical simulations. Examples are shown in Figure 3-26.

It is observed that while the phenomenon of splitting observed in Figure 3-26 a) approximately follows the description given here, the wild splitting giving great separation between the two solitons in Figure 3-26 b) seems to respond to a different effect. Next section as devoted to an intuitive analysis of the phenomenon of radiation emission gives some clues on what are the causes that are likely to lead to such a behavior and in section 6.4 through the results of a series of numerical experiments a systematic study of the splitting phenomenon is carried out.

The mechanism of radiation emission

For a transverse point in the profile to evolve towards its stationary amplitude value it is important to reach quickly the $\Delta\psi \sim 0$ condition and then energy dragging does the rest as providing him and his neighbors with an appropriate amplitude transverse distribution. Less energetic transverse points therefore, as exchanging energy more slowly, find it harder to arrive to the stationary solution and are likely to get stuck around a $\cos(\Delta\psi) < 0$ condition, so that the contribution of the nonlinear terms to the phase is negative. From the transverse points affected by a $\Delta\psi$ value such that $\cos(\Delta\psi) < 0$, more energetic ones as having larger (in absolute value) negative parametric interaction terms experience a greater decrease in their phase constants which causes their energy to result washed away towards other transverse points leading to the creation of amplitude valleys at each side of the peak, see Figure 3-28.

Wild energy exchange produced at the $\cos(\Delta\psi) < 0$ entrance values of $\Delta\psi$, which correspond to energy exchange maxima, prevents more energetic points from being stuck around a $\cos(\Delta\psi) < 0$ value by enhancement rather than correction of the $\Delta\psi$ monotonic tendency so that $\Delta\psi$ is launched over to the next $\cos(\Delta\psi) > 0$ area swiftly crossing the $\cos(\Delta\psi) < 0$ values. See Figures 3-27, 3-28.

Less energetic points which are influenced by the energy exchanges having place inside the $\cos(\Delta\psi) < 0$ values interval, i.e. do not receive a significant impulse to swiftly cross it due to wild energy exchange at its entrance values, can get trapped in these intervals as a consequence of the opposite $\Delta\psi$ evolution tendencies driven by the energy exchange processes at each side of $\Delta\psi = n\pi$, with n an even number.

The transverse area affected by $\cos(\Delta\psi) < 0$ values tend to split from the main profile and travel away from the center as a consequence of negative contribution of nonlinear terms

to the phase by which effect as one transverse point gets energy its phase decreases so that immediately releases the energy it has received towards points with larger phase values.

For typical input fields, by the time the bump appears, the main part of the profile has become very close to the phase locking condition hence holding high phase values just beside the point where the splitting takes place and thus being able through the phase gradient created to recover a great deal of energy trying to get away from main profile and preventing to some extent the radiation of the bump emerged as a consequence of locking around $\cos(\Delta\psi) < 0$.

The process of radiation emission can therefore be understood as a phenomenon of energy escaping away from more energetic $\cos(\Delta\psi) < 0$ transverse areas. If this energy will be recovered by the main profile or else will be radiated apart from it depends basically on the phase gradient created at each side of these $\cos(\Delta\psi) < 0$ areas.

This description of the process of radiation emission explains both the numerics observation of lateral bumps that once created instead of walking away as radiation can in a great proportion join again the main profile, and the messy appearance of radiation which results from this struggling for the energy stored in the most energetic $\cos(\Delta\psi) < 0$ transverse points back and forth between center and tails of the profile.

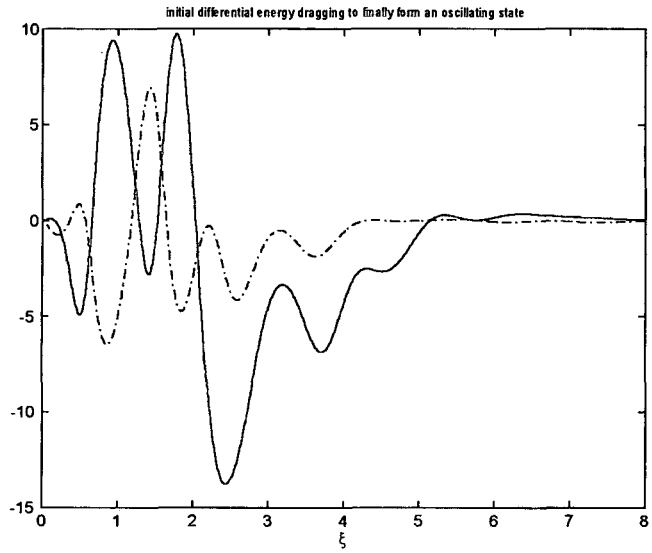

Figure 3-23: Internal energy fluxes of fundamental (-) and second harmonic (-.) at the beams peak for $\beta = 3$, $A_1 = 2$, $A_2 = 1$.

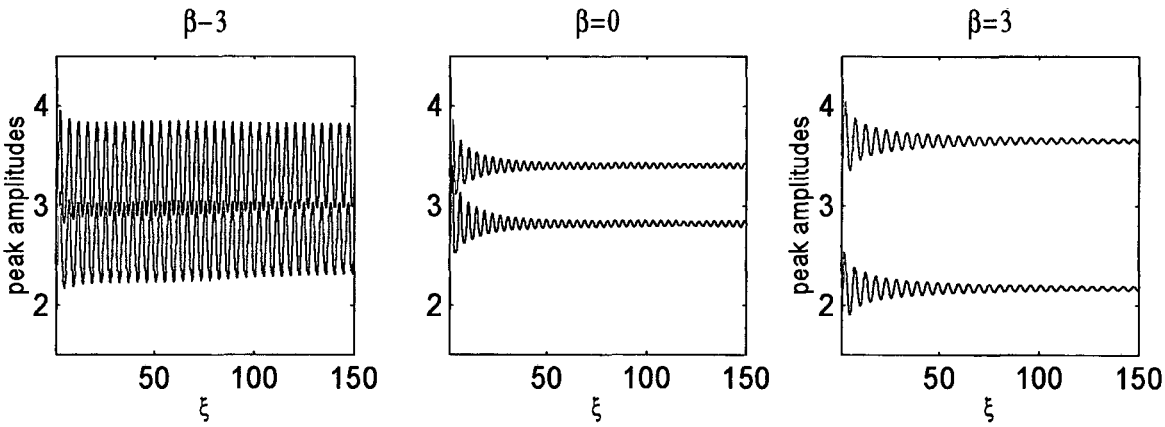

Figure 3-24: Peaks evolution for different values of the wavevector mismatch showing the oscillating nature of the solitary wave formed. In all cases $I = 25$ and the amplitudes have been chosen so as to realize a minimum of hamiltonian.

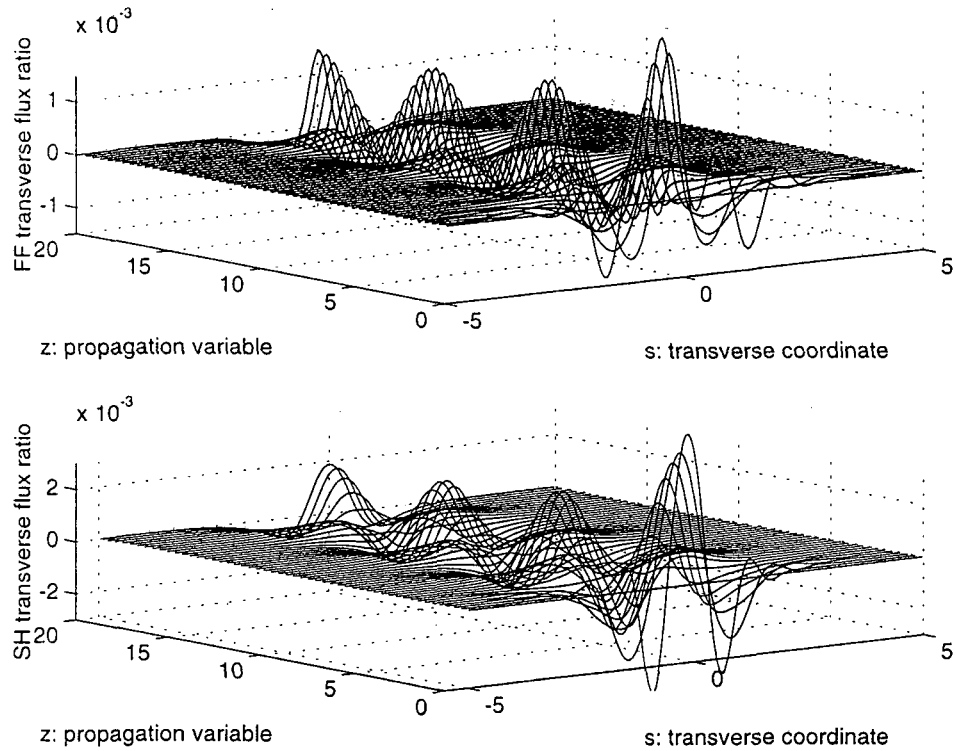

Figure 3-25: Internal energy fluxes generated when the exact analytic solution is propagated using the numerical beam propagation method.

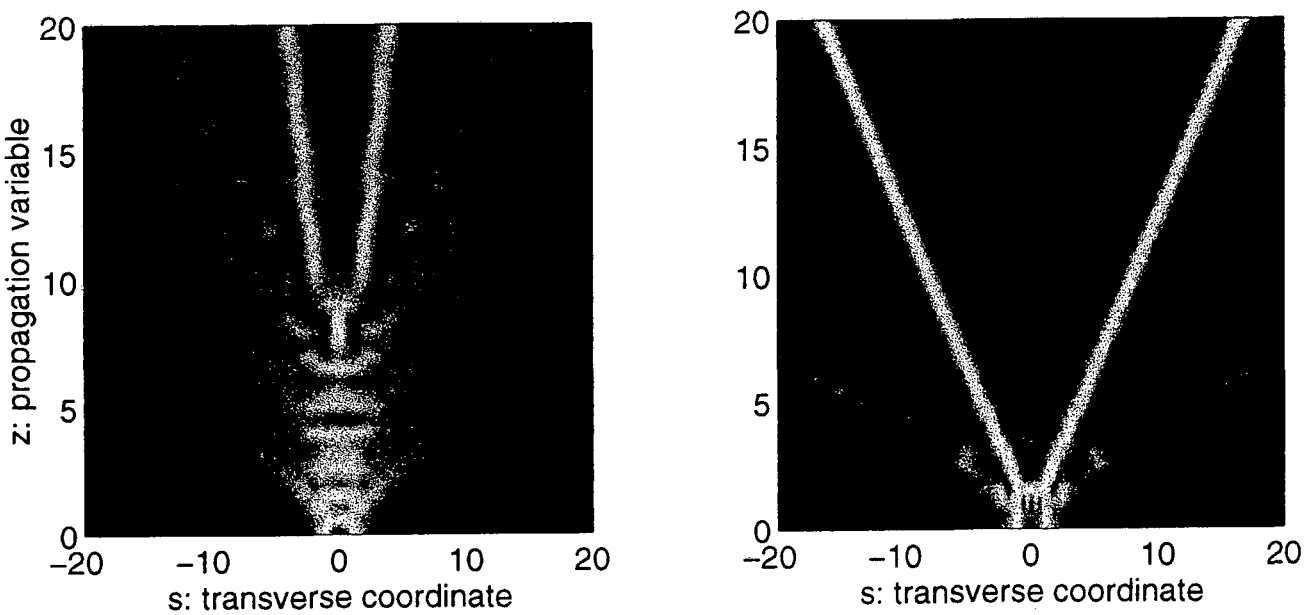

Figure 3-26: Examples of *smooth* (left) and *sharp* splitting. In both cases $\beta = -2$, $A_2 = 0$. Left: $A_1 = 6.5$; right: $A_1 = 10$.

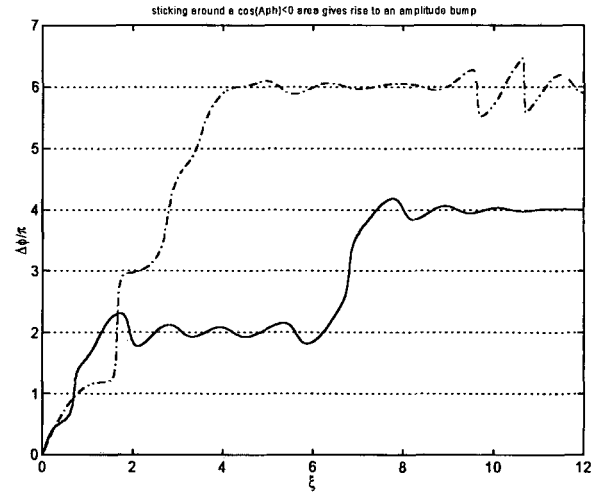

Figure 3-27: Nonlinear phase mismatch evolution at the profiles peak (-) and at $|s| = 1.4$ for $\beta = 3$, $A_1 = 1$, $A_2 = 3$.

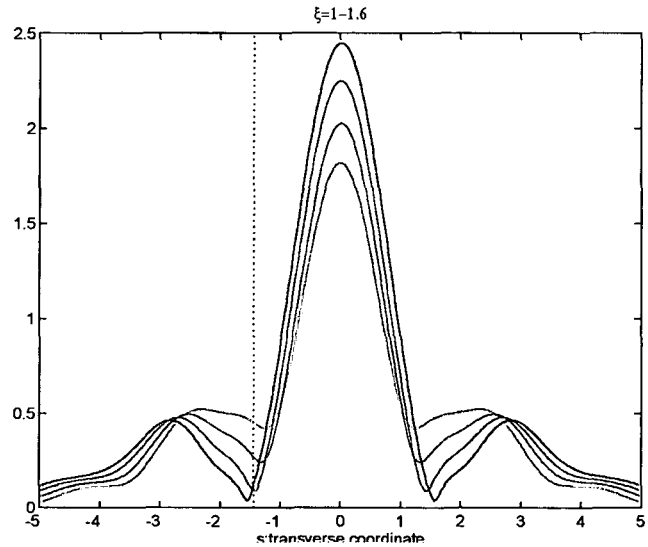

Figure 3-28: Same as previous figure, showing the fundamental transverse profile evolution and the amplitude valley created at $|s| = 1.4$. The propagation variable ξ increases following the sequence 'y', 'm', 'c', 'r', 'g', 'b'. See color scale in Appendix B.

3.7 Summary

After revision of the basic premises to take into account in the search for stationary solutions to the equations governing simultaneous propagation of fundamental and second harmonic beams in a quadratic nonlinear crystal (2.94), and brief explanation of the characteristics of the shooting method, the main properties of the spatial soliton families featuring linear phase fronts and existing in the absence of walk-off have been presented in this chapter. Thanks to the similarity rules enjoyed by the stationary equations (3.22), complete characterization of the families for any value of the wavevector mismatch, β, has only required provision of the characteristics of the families for $\beta = 0$, a positive β value and a negative one.

Worth remarking is the existence of a threshold energy flow scaling as $|\beta|^{3/2}$ for which no solutions are found in $\beta < 0$ cases, whereas solitons exist for all energy flow values in $\beta > 0$ configurations.

Through geometrical considerations based on direct inspection of the $I - \mathcal{H}$ curves defined by the families, it has been shown that most relevant solutions are stable on propagation. The exception is an unstable branch found for near cut-off values in the $\beta < 0$ case.

Analysis of the soliton tails reveals that while the nonlinear phase matching is basically maintained in the $\beta < 0$ case through linear diffraction terms while nonlinear terms tend to zero, for $\beta > 0$, linear terms cancel each other to leave nonlinear phase mismatch cancellation for nonlinear interaction terms, which thus are such that in tails $U_1^2 = \beta U_2$, as in the NLSE limit.

Basic understanding of the main characteristics of the families of stationary solutions is achieved by consideration of maintenance on one side of nonlinear phase matching through equilibrium of interharmonics local energy exchange which thus determines the peaks amplitudes, and on the other, of nonlinear phase constants through linear diffraction terms compensating energy dragging imbalances thus stating the proper transverse distribution. Through the analysis it is seen that as $|\beta|$ is increased broader stationary profiles and higher peak and total energy flow relations (U_1/U_2 and I_1/I_2 respectively) for $\beta > 0$ while lower ones for $\beta < 0$, are encountered. To evaluate the effect that an increase of total energy flow has on the stationary solutions susceptible of being excited, just it is needed to consider that such an increase nonlinearly reduces the effective wavevector mismatch whose nominal value is given by β.

The instability displayed by near threshold $\beta < 0$ solutions is intuitively attributed to too great difference required to cancel nonlinear phase mismatch between exponential decay constants in tails.

Both $I - \mathcal{H}$ planes and Stokes parameters have been used for graphical monitorization of the evolution confirming the robustness of soliton formation for a wide range of system and input conditions from which shown here have been a few interesting cases.

To end up, some remarks about the role played in the evolution by β and the total energy flow, the formation of oscillating states and the mechanism of radiation emission have been included. An increase in $|\beta|$ has been found to basically lead to more and shorter interharmonics energy exchange periods until nonlinear phase matching is achieved while basically an increase of total energy flow reduces the amplitude of nonlinear phase mismatch oscillations.

Energy dragging of different signs is shown to take place into each harmonic in the first stages of propagation until the equilibrium is reached and the oscillating internal energy fluxes follow alternatively the same direction for both harmonics.

Formation of lateral amplitude bumps that eventually result radiated is understood in terms of the intuitive model as energy being dragged away from zones of negative nonlinear parametric interaction causing a decrease in the local phase front values.